



# Zircon U-Pb Age, Geochemical, and Sr-Nd-Pb-Hf Isotopic Constraints on the Time Frame and Origin of Early Cretaceous Mafic Dykes in the Wuling Mountain Gravity Lineament, South China

CHEN Xiaoqing<sup>1,2,\*</sup>, LIU Shen<sup>2</sup>, FENG Caixia<sup>2</sup>, XU Jingyan<sup>2</sup>, ZHAO Huibo<sup>2</sup>, FENG Guangying<sup>3</sup>, Ian M. COULSON<sup>4</sup>, SUN Jingui<sup>1</sup> and FAN Yan<sup>2</sup>

<sup>1</sup> College of Earth Sciences, Jilin University, Changchun 130061, China

<sup>2</sup> State Key Laboratory of Continental Dynamics and Department of Geology, Northwest University, Xi'an 710069, China

<sup>3</sup> Institute of Geology, Chinese Academy of Geological Sciences, Beijing 100037, China

<sup>4</sup> Solid Earth Studies Laboratory, Department of Geology, University of Regina, Regina, Saskatchewan S4S 0A2, Canada

**Abstract:** In view of the importance of mafic dyke swarms and their contribution to current scientific problems relating to South China, herein, we present the findings of studies on twenty-five representative mafic dykes cropping out in Hunan Province and Guangxi Zhuang Autonomous Region, within the southern Wuling Mountain gravity lineament, China. These results include new zircon LA-ICP-MS U-Pb age, whole rock geochemical, Sr-Nd-Pb isotopic, and zircon Hf isotopic data for these dykes. The dykes formed between  $131.5 \pm 1.2$  and  $121.6 \pm 1.1$  Ma, and have typical doleritic textures. They fall into the alkaline and shoshonitic series, are enriched in light rare earth elements (LREE), some large ion lithophile elements (LILE; e.g., Rb, Ba, and Sr), Th, U, and Pb, and are depleted in Nb, Ta, Hf, and Ti. Moreover, the dolerites have high initial  $^{87}\text{Sr}/^{86}\text{Sr}$  ratios (0.7055–0.7057), negative  $\varepsilon_{\text{Nd}}(t)$  and zircon  $\varepsilon_{\text{Hf}}(t)$  values (–14.8 to –11.9, –30.4 to –14.9), and relatively constant initial Pb isotopic ratios (that are EM1-like, 16.77–16.94, 15.43–15.47, and 36.84–36.92 for  $^{206}\text{Pb}/^{204}\text{Pb}$ ,  $^{207}\text{Pb}/^{204}\text{Pb}$ , and  $^{208}\text{Pb}/^{204}\text{Pb}$ , respectively). These results indicate that the dykes were likely derived from magma generated through low-degree partial melting (1.0%–10%) of an EM1-like garnet–lherzolite mantle source. The parental magmas fractionated olivine, clinopyroxene, plagioclase, and Ti-bearing phases with negligible crustal contamination, during ascent and dyke emplacement. Several possible models have been proposed to explain the origin of Mesozoic magmatism along the Wuling Mountain gravity lineament. Herein we propose a reasonable model for the origin of these mafic dykes, involving the collision between the paleo-Pacific Plate and South China, which led to subsequent lithospheric extension and asthenosphere upwelling, resulting in partial melting the underlying mantle lithosphere in the Early Cretaceous, to form the parental magmas to the WMGL mafic dykes, as studied.

**Key words:** mafic dykes, magmatic origin, Early Cretaceous, Wuling Mountain gravity lineament, South China

Citation: Chen et al., 2021. Zircon U-Pb Age, Geochemical, and Sr-Nd-Pb-Hf Isotopic Constraints on the Time Frame and Origin of Early Cretaceous Mafic Dykes in the Wuling Mountain Gravity Lineament, South China. *Acta Geologica Sinica (English Edition)*, 95(2): 419–438. DOI: 10.1111/1755-6724.14656

## 1 Introduction

The Wuling Mountain gravity lineament (WMGL) is one of the most important NNE-trending tectonic zones in China (Zhou and Liu, 1979; Ma, 1987; Yang, 1988; Liu et al., 2003; Cai et al., 2004; Ma et al., 2006), delineating a continental margin and zone of deep crustal folding (Khan, 1976; Cochran and Talwani, 1977; Zeng, 1984; Ma and Sun, 1987; Ren et al., 1992; Liu, 1994), this lineament is some 3,700 km long and 8–200 km wide, encompassing an area of ~21,000 km<sup>2</sup>. Previous studies have shown that the WMGL plays host to a large number of Mesozoic extensional and faulted basins (Du et al., 1999; Shao, 2001; Deng et al., 2003; Bai et al., 2007; Zhang et al., 2012; Luo et al., 2014), detachment fault and metamorphic

core complexes (Shen et al., 2008; Zhang et al., 2012; Ji, 2014), graben horst (Li and Yang, 1988; Chen, 2013), rift (Wu et al., 1985; Deng et al., 2003; Bai et al., 2007; Zhang et al., 2013), basin ridge structures (Shu et al., 2004; Bai et al., 2005; Shu, 2012), and normal faulting (Zhang et al., 2012). Further, that igneous activity within this zone of tectonism includes: A-type and high-potassium I-type granites (Li, 2000; Zhou, 2003; Wang, 2004; Wang et al., 2005a; Bai et al., 2007), adakite and bi-modal suite volcanic rocks (Li, 2000; Zhou, 2003; Bai et al., 2007), and a widely distributed mafic dyke swarms (Li, 2000; Jia et al., 2002a, b, c; Jia, 2003; Zhou, 2003; Fan et al., 2003; Wang et al., 2008); the lineament also is a region rich economic mineral deposits (Tu et al., 1998, 2000; Mao et al., 2004, 2009; Chen et al., 2014; Hu et al., 2015). These geological phenomena and studies have demonstrated that an important period of lithospheric extension affected the

\* Corresponding author. E-mail: xqchen66@163.com

WMGL during the Mesozoic (Li, 2000; Wu et al., 2008). Nevertheless, the temporal and spatial distribution of lithospheric extension is still at present unclear. Moreover, the investigation of Mesozoic magmatism in the WMGL is limited to some intermediate–felsic igneous rocks (e.g., granite, volcanic rock and adakite; Yan and Ye, 1982; Zhang, 1986, 2010; Mao et al., 2014; Huang et al., 2014), the mantle properties and the genetic model for these extensional-related igneous activities are poorly.

In addition to the above-mentioned scientific problems, since the assembly of the Indosinian plate, the South China block has resided in the interior of a continent, and its evolution has been influenced by the interaction of adjacent plates, that provide for a complex tectonic framework to this part of Asia. Earlier studies have shown that, as a representative geological tectonic belt of South China Block, the Mesozoic lithospheric extension of the WMGL occurred intensively; however, the temporal and spatial distribution law, dynamic mechanism and tectonic setting resulting in this stretching is as yet unresolved (Molnar and Tapponnier, 1975; Tapponnier and Molnar, 1976; Hilde et al., 1977; Huang and Fu, 1982; Wang et al., 1990; Wan, 1993; Wang et al., 1996; Yang et al., 1996; Yang and Liu, 2000; Niu, 2005; Xu, 2006; Huang et al., 2008; Ge et al., 2014). Therefore, in order to help resolve these uncertainties, it is necessary to select suitable research areas to focus upon in further research on the WMGL. As representatives of magmatism that may accompany episodes of lithospheric extension, mafic dyke swarms are a series of linear, hypabyssal intrusions of mafic igneous rock (e.g., dolerite/gabbro, diorite and, more rarely, lamprophyre) (Halls, 1982; Zhou et al., 1987; Gilder et al., 1991; Ernst et al., 1995; Li et al., 1997, 2001; Shao and Zhang, 2002; Jia, 2003; Xie, 2003; Liu, 2004; Li et al., 2005; Liu et al., 2008a, b, 2009, 2017, 2018; Zhao, 2004; Zhao et al., 2004; Peng et al., 2005, 2007, 2008, 2010, 2011a, b; Hou et al., 2006, 2016; Zhang, 2006; Feng et al., 2012; Yang, 2012; Qi et al., 2016). Mafic dyke swarms mainly distribute in North America, Brazil, Baltic Sea, Australia, Siberia, South Africa, Zimbabwe, India, Greenland, Scotland, Qinghai Province, Xinjiang Uygur Autonomous Region, Tarim Basin, Tibet Autonomous Region, Eastern China and the North China Craton (NCC) (Zhou, 1987; Wang and Rao, 1989; Hou and Mu, 1994; Li et al., 1997; Zhou et al., 1997; Li, 2000; Li et al., 2001; Jia et al., 2002a, b, c; Xie et al., 2002; Shao and Zhang, 2002; Jia, 2003; Xie, 2003; Zhai and Liu, 2003; Hai and Liu, 2003; Liu, 2004; Liu et al., 2008a, b, 2009, 2017, 2018; Zhao, 2004; Zhao et al., 2004; Yang et al., 2004; Shao et al., 2005; Peng et al., 2005, 2007, 2008, 2010, 2011a, b; Feng et al., 2012; Qi et al., 2012, 2016; Yang, 2012; Hou, 2012; Yang et al., 2013; Hou et al., 2006; Feng et al., 2012; Yang et al., 2013; Zhang et al., 2019a, b; Feng et al., 2020). The presently accepted age range for this style of magmatism is mainly between 2.4 Ga and 2.1 Ga; more recent mafic dyke swarms emplaced in the Phanerozoic are chiefly concentrated in the period 230–40 Ma (Li et al., 1997; Zhai and Liu, 2003; Shao et al., 2005).

Our present understanding of mafic dyke swarm and their significance is that these provide an important window in to the deep lithosphere and mantle source

regions for the magmas; this mafic magma also can inform about the dynamic conditions attending melting in the lower crustal/upper mantle in response to stretching (Liu et al., 2010a; Lin et al., 2014). As such, studies of swarms of mafic dykes may give key scientific insight into the evolution of major crustal blocks, including processes of accretion and reconstruction, the temporal and spatial controls on lithospheric extension, as well as to mantle properties and the genetic model for magmatism under an extensional background, and any role this has in large-scale mineralization (Halls, 1982; Halls and Fahrig, 1987; Zhou, 1987; Ernst et al., 1995; Li et al., 1997; Zhou et al., 1997, 2001; Li, 2000; Shao and Zhang, 2002; Liu, 2004; Mao et al., 2004; Zhao et al., 2004; Hou et al., 2005; Liu et al., 2008a, b, 2009, 2017, 2018; Hou, 2012; Hu et al., 2007, 2015; Gao et al., 2019). At present, Chinese researchers have mainly focused on Mesozoic intraplate mafic dyke swarms in eastern China and those within the NCC (Zhou et al., 1987; Hou and Mu, 1994; Li et al., 1997; Shao and Zhang, 2002; Xie et al., 2003; Jia, 2003; Xie, 2003; Hai and Liu, 2003; Liu, 2004; Zhao, 2004; Yang et al., 2004; Shao et al., 2005; Liu et al., 2008a, b, 2009, 2017, 2018; Peng et al., 2005, 2007, 2008, 2010, 2011a, b; Hou et al., 2006, 2016; Feng et al., 2012; Yang, 2012; Yang et al., 2013). By contrast, the study of Mesozoic mafic dyke swarms in other geological tectonic belts within China (e.g., the WMGL) is poor. To address these deficiencies and the above-mentioned scientific problems, we herein have chosen to directly study examples of Mesozoic magmatism as recorded in mafic dyke swarms from the Hunan Province and Guangxi Zhuang Autonomous Region within the southern WMGL. Our studies of the dykes include U-Pb geochronology, whole-rock geochemistry and Sr-Nd-Pb-Hf isotopes.

## 2 Geological Setting and Dyke Petrology

As the southern segment of the Greater Hinggan Mountains–Taihang Mountains–Wuling Mountains gravity lineament (Cochran and Talwani, 1977; Zhou and Liu, 1979; Zeng, 1984; Ma and Dun, 1987; Ma, 1987; Yang, 1988; Ren et al., 1992; Liu et al., 1994, 2003; Cai et al., 2004; Yang et al., 2005; Ma et al., 2006), the WMGL extends northwards to the Russian Far East, south to Vietnam and Laos, and spans the Henan, Hubei, Hunan, Guizhou provinces and the Guangxi Autonomous Region of China. The spatial distribution of Mesozoic magmatism in South China encompasses not only granitoids and mafic dykes, but also sequences of volcanic–intrusive rocks; principal lithologies include intermediate–felsic intrusive rocks and their volcanic equivalents (Zhang, 1986). Geochronological constraints for the Triassic and middle Jurassic granitoids find that in the area of Qin–Hangzhou Mid–Jurassic to Early Cretaceous volcanic–intrusive suites predominate (175–123 Ma), whereas in the middle and lower reaches of the Yangtze River, Late Jurassic to Early Cretaceous volcanic–intrusive units occur (145–123 Ma). Late Jurassic to Late Cretaceous (145–85 Ma) volcanic–intrusive suites also occur along the southeastern coast and Early Jurassic volcanic–intrusive rock zone (200–180 Ma). Moreover, the magmatic activity is

characterized by multi-stage, SW–NW facing and/or zonal patterns (Mao et al., 2014). As a good representative of Mesozoic magmatism in South China, the spatial distribution of magmatic activity within the WMGL spans from 110°8' to 112°15' in the East (longitude) and 23°55' to 34°33' in the North (latitude). The timing of igneous activity along the WMGL is chiefly concentrated in the Jurassic and Cretaceous, with the magma types including examples of various granite(s), granodiorite, monzonite, diorite, gabbro/dolerite and lamprophyre.

Our present study includes 25 representative samples collected from mafic dyke swarm across from five areas (i.e., the Guzhang, Jishou, Yuanling, Donglan, Baise, and Yixian) within the Hunan Province and Guangxi Zhuang Autonomous Region, southern WMGL, China (Fig. 1). Individual mafic dykes studied were observed as near vertical, striking ~NE–SW, with widths in excess of 10 m and lengths of the order 0.8–15 km (Fig. 1); each have typical doleritic textures. The study area encompasses a Proterozoic complex, and sequences of Sinian/Neoproterozoic, Ordovician, Silurian, Devonian, Carboniferous, Permian, Triassic, Jurassic, and Cretaceous sedimentary rock, and local granite and monzonite that are all intruded by the mafic dykes during the Mesozoic (Fig. 1; BGMRGZAR, 1985; BGMRHP, 1988). The mafic dykes studied are typical dolerites, having a combined phenocryst content of ~30%–35%, chiefly comprising clinopyroxene, plagioclase, and minor biotite (0.5–1.3 mm). The groundmass (60%–65%) plays host also to pyroxene, plagioclase, and magnetite (+/- chlorite).

### 3 Analytical Procedures

#### 3.1 U-Pb dating by LA-ICP-MS methods

Zircon grains from five of the investigated mafic dyke samples from the southern segment of the WMGL, in the areas of Hunan Province and Guangxi Zhuang

Autonomous Region, were separated using conventional heavy liquid and magnetic techniques. Representative zircon were then handpicked under a binocular microscope before being mounted in an epoxy resin disc, polished, and then coated with gold prior to analysis. These zircon crystals were imaged using both transmitted and reflected light microscopy, and by means of cathodoluminescence (CL) to help in their characterization, and to reveal their internal structure. The CL imaging and U-Pb analysis were undertaken at the State Key Laboratory of Continental Dynamics, Northwest University, China. The analytical procedures used were those described in detail in Harris et al. (2004); a spot diameter of 29  $\mu$ m was used. U-Th-Pb ratios and absolute abundances were determined by reference to multiple measurements of a standard TEMORA zircon and the NIST 610 glass standard.

#### 3.2 Major elemental and trace elemental analyses

Major element compositions were determined using an analytical Axioms-advanced X-ray fluorescence spectrometer at the State Key Laboratory of Ore Deposit Geochemistry (LODG), Institute of Geochemistry, Chinese Academy of Sciences, Guiyang, using fused lithium tetra borate glass pellets. This analysis has an analytical precision of better than 5%. Trace element compositions were determined by Inductively-coupled plasma mass-spectrometry (ICP-MS) and a Perkin-Elmer ELAN DRC-e instrument at the LODG, Guiyang. Prior to analysis, powdered samples (50 mg) were dissolved in high-pressure Teflon bombs, using an HF + HNO<sub>3</sub> attack for 48 hours at about 190°C (Qi et al., 2000). Signal drift during analysis was monitored using Rh as an internal standard, and GBPG-1, OU-6, GSR-1, and GSR-3 standards were used for analytical quality control, indicating an analytical precision that is generally better than 5% for all trace elements.

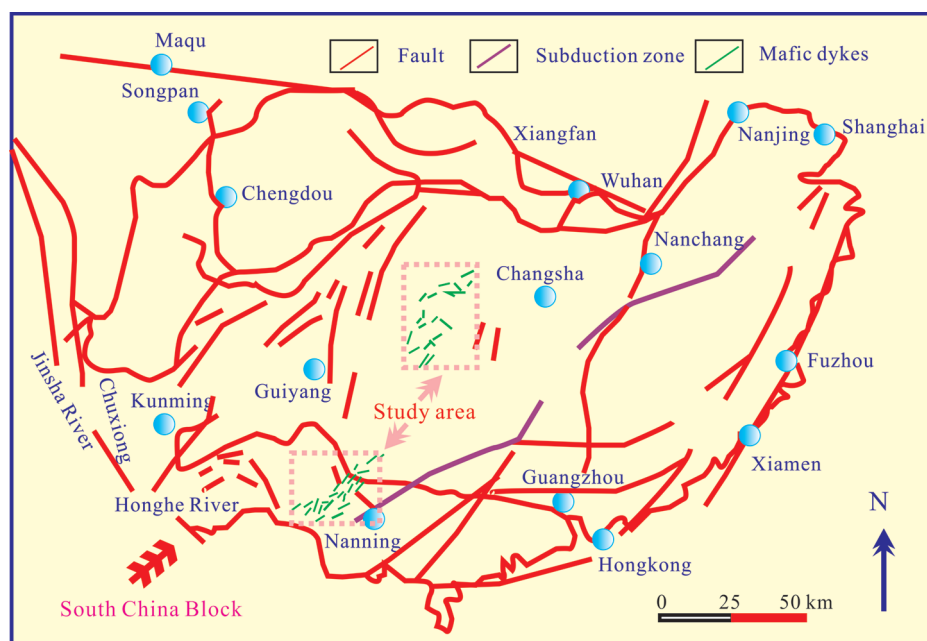


Fig. 1. Schematic illustration showing the distribution of the mafic dykes in the WMGL.

### 3.3 Sr-Nd-Pb isotopic analyses

For Rb-Sr and Sm-Nd isotope analyses, sample powders were spiked with mixed isotope tracers, dissolved in Teflon capsules with HF + HNO<sub>3</sub> acids, and separated by conventional cation-exchange techniques (Zhang et al., 2001). Isotopic measurements were performed using a Finnigan Triton Ti thermal ionization mass spectrometer at the LODG, Guiyang. Procedural blanks yielded concentrations of < 200 pg for Sm and Nd and < 500 pg for Rb and Sr, whilst mass fractionation corrections for Sr and Nd isotopic ratios were based on <sup>86</sup>Sr/<sup>88</sup>Sr = 0.1194 and <sup>146</sup>Nd/<sup>144</sup>Nd = 0.7219, respectively. Analysis of the NBS987 and La Jolla standards yielded values of <sup>87</sup>Sr/<sup>86</sup>Sr = 0.710246 ± 16 (2σ), and <sup>143</sup>Nd/<sup>144</sup>Nd = 0.511863 ± 8 (2σ), respectively. Prior to Pb isotopic analysis, Pb was separated and purified by conventional cation-exchange techniques using diluted HBr as an eluent. Analysis of the NBS981 standard yielded a mean <sup>204</sup>Pb/<sup>206</sup>Pb value of 0.0895 ± 15, a mean <sup>207</sup>Pb/<sup>206</sup>Pb value of 0.9146 ± 8, and a mean <sup>208</sup>Pb/<sup>206</sup>Pb value of 2.163 ± 2.

### 3.4 In situ zircon Hf isotopic analysis

In situ, zircon Hf isotopic analyses were undertaken using a multi-collector-inductively coupled plasma-mass spectrometer (MC-ICP-MS) instrument equipped with a Geolas-193 laser, at the Key Laboratory of Continental Dynamics, Northwest University, China. These analyses used a laser repetition rate of 10 Hz at 100 mJ and a beam diameter of either 32 or 63 mm. The isobaric interference of <sup>176</sup>Lu on <sup>176</sup>Hf was corrected by measuring the intensity of the interference-free <sup>175</sup>Lu isotope and using a recommended <sup>176</sup>Lu/<sup>175</sup>Lu ratio of 0.02655 (Machado and Simonetti, 2001). A <sup>176</sup>Yb/<sup>172</sup>Yb value of 0.5887 (Chu et al., 2002) and mean *b<sub>Yb</sub>* values obtained during Hf analysis were used to correct for the interference of <sup>176</sup>Yb on <sup>176</sup>Hf (Iizuka and Hirata, 2005). Details of the analytical and data correction procedures are given in Wu et al. (2006). Our analyses included measurements of standard 91500 and FM0411 zircons, yielding mean <sup>176</sup>Hf/<sup>177</sup>Hf ratios of 0.282312 ± 36 (2 standard deviations (2 SD), *n* = 35) and 0.282995 ± 31 (2 SD, *n* = 9), respectively, which agree with the reported <sup>176</sup>Hf/<sup>177</sup>Hf composition of the 91500 zircon (0.282305 ± 8, 2 SD, *n* = 30) as determined by solution analysis (Woodhead et al., 2004) and 0.282983 ± 17 (2 SD, *n* = 9) for the FM0411 zircon by in situ analytical methods (Wu et al., 2006).

## 4 Results

### 4.1 Zircon U-Pb geochronology

Euhedral zircon grains in samples GZ01, JS02, YL01, DL02, and BS01 were observed to be clean and prismatic, with evident oscillatory zoning, suggestive that these were the products of magmatic crystallization. A total of 11 zircon grains provided a weighted mean <sup>206</sup>Pb/<sup>238</sup>U age of 128 ± 1.2 Ma (1σ) (95% confidence interval, MSWD = 0.104) for GZ01; 11 zircon grains gave a weighted mean <sup>206</sup>Pb/<sup>238</sup>U age of 127.6 ± 1.1 Ma (1σ) (95% confidence interval, MSWD = 0.27) for JS02; 11 grains gave a weighted mean <sup>206</sup>Pb/<sup>238</sup>U age of 131.5 ± 1.2 Ma (1σ) (95% confidence interval, MSWD = 0.14) for YL01; 12

grains have a weighted mean <sup>206</sup>Pb/<sup>238</sup>U age of 121.6 ± 1.1 Ma (1σ) (95% confidence interval, MSWD = 0.54) for DL02, and 12 grains provided a weighted mean <sup>206</sup>Pb/<sup>238</sup>U age of 121.8 ± 1.4 Ma (1σ) (95% confidence interval, MSWD = 0.27) for BS01 (Table 1; Fig. 2). These determinations are the best estimates of the crystallization age of the mafic/dolerite dykes studied. And there were no inherited characteristics observed in the studied WMGL zircon.

### 4.2 Major and trace elements

Whole-rock geochemical data for the mafic dykes of the study areas are presented in Tables 2 and 3; the samples include representatives of dolerite. The dolerite samples exhibit a fairly narrow range of compositions, SiO<sub>2</sub> (50.14 wt%–51.86 wt%), TiO<sub>2</sub> (0.96 wt%–1.33 wt%), Al<sub>2</sub>O<sub>3</sub> (15.82 wt%–16.54 wt%), Fe<sub>2</sub>O<sub>3</sub> (7.37 wt%–9.66 wt%), MnO (0.13 wt%–0.18 wt%), MgO (5.06 wt%–6.63 wt%), CaO (6.88 wt%–7.94 wt%), Na<sub>2</sub>O (2.83 wt%–3.15 wt%), K<sub>2</sub>O (2.66 wt%–3.68 wt%), P<sub>2</sub>O<sub>5</sub> (0.45 wt%–1.26 wt%), and a relatively small loss of ignition (LOI, 0.78–2.36) (Table 2). All samples fall into the alkaline field in terms of the total alkali–silica (TAS) diagram (Fig. 3a), and the shoshonitic field for the Na<sub>2</sub>O vs. K<sub>2</sub>O plot (Fig. 3b). The mafic dykes studied display regular trends of decreasing CaO, Al<sub>2</sub>O<sub>3</sub>, and MgO (Fig. 4b, e), however, irregular correlation between SiO<sub>2</sub>, TiO<sub>2</sub>, Na<sub>2</sub>O, K<sub>2</sub>O, Fe<sub>2</sub>O<sub>3</sub>, P<sub>2</sub>O<sub>5</sub>, and MgO (Fig. 4a, c–h) was observed. The samples are also characterized by LREE enrichment and HREE depletion, with a wide range in ratios (20–37.8) and Eu/Eu\* (0.62–0.95) (Table 3 and Fig. 5a, b). On primitive mantle-normalized trace element diagrams, the dolerite rocks show enrichment in LILEs (i.e., Rb, Ba, Th, U, Pb, and Sr) and depletion in HFSEs (i.e., Nb, Ta, Hf, and Ti) (Fig. 5b).

### 4.3 Sr-Nd-Pb isotopes

Sr, Nd, and Pb isotopic data for 25 representative mafic dyke samples are presented in Table 4, 5 and; Figs. 6, 7a, b. The investigated dolerites show very similar (<sup>87</sup>Sr/<sup>86</sup>Sr)<sub>i</sub> values, ranging from 0.7055 to 0.7057, and wide variation in ε<sub>Nd</sub>(*t*) values, from –11.9 to –14.8, which suggest an enriched source region. In addition, the dolerites have relatively constant Pb isotopic ratios that are Em1-like ((<sup>206</sup>Pb/<sup>204</sup>Pb)<sub>i</sub> = 16.77–16.94, (<sup>207</sup>Pb/<sup>204</sup>Pb)<sub>i</sub> = 15.43–15.47, and (<sup>208</sup>Pb/<sup>204</sup>Pb)<sub>i</sub> = 36.84–36.92).

### 4.4 Zircon Hf isotopes

Five samples of the zircon dated by U-Pb methods were further analyzed for their Lu-Hf isotopic compositions, with results presented in Table 6. Sixteen spot analyses were determined for the zircon within sample GZ01, yielding variable ε<sub>Hf</sub>(*t*) values of between –16.6 and –18.4 (Table 6; Figs. 8, 9a, b). These provide for a one-stage model age (*T*<sub>DM1</sub>) between 1,444 and 1523 Ma (Table 6), and give initial <sup>176</sup>Hf/<sup>177</sup>Hf ratios ranging from 0.2812176 to 0.282225. Nineteen spot analyses were obtained for the zircon within JS02, yielding variable ε<sub>Hf</sub>(*t*) values of between –15.2 and –18.0 (Table 6; Fig. 8c, d), one-stage model ages (*T*<sub>DM1</sub>) between 1,380 and 1,542 Ma (Table 6; Fig. 8c, d), and initial <sup>176</sup>Hf/<sup>177</sup>Hf ratios of 0.282183 to 0.282265. Seventeen spot analyses were obtained for

**Table 1** LA-ICP-MS U-Pb isotopic data of zircon separated from the mafic dykes studied of the Wuling Mountain gravity lineament

GZ01				Isotopic ratios						Age (Ma)						
Spot	Pb (ppm)	Th (ppm)	U (ppm)	Th/U	$^{207}\text{Pb}/^{206}\text{Pb}$	$1\sigma$	$^{207}\text{Pb}/^{235}\text{U}$	$1\sigma$	$^{206}\text{Pb}/^{238}\text{U}$	$1\sigma$	$^{207}\text{Pb}/^{206}\text{Pb}$	$1\sigma$	$^{207}\text{Pb}/^{235}\text{U}$	$1\sigma$	$^{206}\text{Pb}/^{238}\text{U}$	$1\sigma$
1.1	15.4	196	153	1.3	0.0493	0.0043	0.1359	0.0118	0.0200	0.0004	159	196	128	10.5	128	2.78
2.1	12.8	172	125	1.4	0.0494	0.0027	0.1362	0.0068	0.0201	0.0003	165	122	129	6.18	128	1.86
3.1	13.6	195	141	1.4	0.0535	0.0034	0.1495	0.0091	0.0203	0.0004	352	136	142	7.93	128	2.22
4.1	14.4	188	144	1.3	0.0468	0.0033	0.1286	0.0086	0.0198	0.0003	48	161	122	7.85	127	2.21
5.1	13.3	204	153	1.3	0.0502	0.0026	0.1398	0.0070	0.0202	0.0003	208	122	132	6.22	129	1.86
6.1	12.8	165	138	1.2	0.0526	0.0028	0.1457	0.0072	0.0201	0.0003	313	116	137	6.45	128	1.92
7.1	17.5	282	196	1.4	0.0459	0.0025	0.1272	0.0062	0.0202	0.0003	0	113	122	5.55	128	1.83
8.1	13.9	147	127	1.2	0.0498	0.0031	0.1391	0.0081	0.0202	0.0003	186	141	131	7.22	129	2.06
9.1	13.2	175	133	1.3	0.0516	0.0035	0.1430	0.0091	0.0201	0.0004	266	146	136	8.05	128	2.24
10.1	19.4	262	198	1.3	0.0465	0.0028	0.1279	0.0072	0.0199	0.0004	29	138	121	6.45	127	1.93
11.1	13.7	196	155	1.3	0.0516	0.0036	0.1428	0.0092	0.0201	0.0004	343	176	166	10.8	128	2.36
JS02																
Spot	Pb (ppm)	Th (ppm)	U (ppm)	Th/U	$^{207}\text{Pb}/^{206}\text{Pb}$	$1\sigma$	$^{207}\text{Pb}/^{235}\text{U}$	$1\sigma$	$^{206}\text{Pb}/^{238}\text{U}$	$1\sigma$	$^{207}\text{Pb}/^{206}\text{Pb}$	$1\sigma$	$^{207}\text{Pb}/^{235}\text{U}$	$1\sigma$	$^{206}\text{Pb}/^{238}\text{U}$	$1\sigma$
1.1	43.2	665	468	1.4	0.0532	0.0038	0.1292	0.0035	0.0198	0.0002	343	159	136	9.08	128	2.53
2.1	46.4	754	489	1.5	0.0483	0.0021	0.1332	0.0050	0.0201	0.0003	115	96.6	128	4.53	127	1.68
3.1	21.6	375	253	1.5	0.0482	0.0022	0.1345	0.0055	0.0203	0.0003	106	103	128	4.86	129	1.72
4.1	38.4	702	485	1.4	0.0496	0.0021	0.1378	0.0049	0.0202	0.0003	181	91.5	131	4.38	128	1.65
5.1	34.3	646	438	1.5	0.0488	0.0022	0.1335	0.0055	0.0198	0.0003	142	103	128	4.92	127	1.71
6.1	38.1	705	482	1.5	0.0473	0.0015	0.1292	0.0038	0.0198	0.0002	61.2	80.3	123	3.41	128	1.52
7.1	34.5	358	312	1.1	0.0472	0.0016	0.1292	0.0036	0.0198	0.0003	861	115	195	9.65	127	2.55
8.1	28.4	526	345	1.5	0.0465	0.0021	0.1378	0.0053	0.0198	0.0003	94.8	166	127	8.55	127	2.45
9.1	51.4	826	614	1.3	0.0465	0.0022	0.1375	0.0052	0.0198	0.0003	25.5	105	122	4.74	127	1.73
10.1	73.3	1084	853	1.3	0.0498	0.0018	0.1378	0.0032	0.0202	0.0003	165	64.8	132	2.76	128	1.45
11.1	32.3	552	384	1.4	0.0476	0.0015	0.1292	0.0036	0.0196	0.0002	0.2	44.5	122	5.92	127	1.98
YL01																
Spot	Pb (ppm)	Th (ppm)	U (ppm)	Th/U	$^{207}\text{Pb}/^{206}\text{Pb}$	$1\sigma$	$^{207}\text{Pb}/^{235}\text{U}$	$1\sigma$	$^{206}\text{Pb}/^{238}\text{U}$	$1\sigma$	$^{207}\text{Pb}/^{206}\text{Pb}$	$1\sigma$	$^{207}\text{Pb}/^{235}\text{U}$	$1\sigma$	$^{206}\text{Pb}/^{238}\text{U}$	$1\sigma$
1.1	19.5	246	195	1.3	0.0495	0.0026	0.1419	0.0065	0.0206	0.0004	182	112	136	5.72	132	1.82
2.1	18.4	185	152	1.2	0.0487	0.0025	0.1378	0.0055	0.0206	0.0004	651	193	168	14.5	131	3.43
3.1	16.3	228	163	1.4	0.0485	0.0023	0.1376	0.0056	0.0204	0.0003	755	105	182	7.58	132	2.08
4.1	13.7	186	144	1.3	0.0518	0.0026	0.1416	0.0068	0.0205	0.0003	278	115	141	6.16	132	1.86
5.1	12.5	144	113	1.3	0.0496	0.0024	0.1418	0.0065	0.0206	0.0003	255	123	143	6.71	131	2.02
6.1	13.3	145	122	1.2	0.0475	0.0025	0.1338	0.0068	0.0205	0.0003	68	125	128	6.06	130	1.91
7.1	14.6	186	147	1.3	0.0488	0.0027	0.1371	0.0072	0.0205	0.0003	135	125	132	6.38	131	1.88
8.1	22.4	338	242	1.4	0.0484	0.0021	0.1378	0.0055	0.0208	0.0003	112	102	130	4.86	132	1.73
9.1	11.4	136	108	1.3	0.0452	0.0028	0.1378	0.0055	0.0206	0.0003	11.00	98	125	6.96	131	2.08
10.1	16.5	252	183	1.4	0.0502	0.0025	0.1422	0.0065	0.0206	0.0004	505	186	155	12.3	132	3.03
11.1	19.8	275	234	1.2	0.0486	0.0022	0.1378	0.0056	0.0205	0.0003	136	105	131	5.03	132	1.73
DL02																
Spot	Pb (ppm)	Th (ppm)	U (ppm)	Th/U	$^{207}\text{Pb}/^{206}\text{Pb}$	$1\sigma$	$^{207}\text{Pb}/^{235}\text{U}$	$1\sigma$	$^{206}\text{Pb}/^{238}\text{U}$	$1\sigma$	$^{207}\text{Pb}/^{206}\text{Pb}$	$1\sigma$	$^{207}\text{Pb}/^{235}\text{U}$	$1\sigma$	$^{206}\text{Pb}/^{238}\text{U}$	$1\sigma$
1.1	9.26	138	105	1.3	0.0496	0.0037	0.1303	0.0096	0.0191	0.0004	188	166	125	8.6	121	2.18
2.1	12.6	168	135	1.2	0.0498	0.0028	0.1322	0.0076	0.0195	0.0003	191	131	128	6.5	123	1.88
3.1	18.4	336	232	1.4	0.0535	0.0025	0.1335	0.0076	0.0188	0.0003	345	103	131	5.26	121	1.68
4.1	22.5	355	268	1.3	0.0495	0.0026	0.1298	0.0066	0.0191	0.0003	175	121	125	5.92	120	1.83
5.1	14.5	164	132	1.2	0.0515	0.0031	0.1335	0.0075	0.0188	0.0003	261	135	128	6.76	121	1.95
6.1	15.4	195	156	1.3	0.0496	0.0032	0.1319	0.0078	0.0194	0.0003	222	155	130	8.05	123	2.24
7.1	23.8	355	262	1.4	0.0483	0.0032	0.1285	0.0085	0.0193	0.0003	115	155	124	7.56	123	2.15
8.1	13.8	158	135	1.2	0.1312	0.0048	0.1296	0.0065	0.0192	0.0003	2115	64	305	8.03	120	1.81
9.1	21.3	366	264	1.4	0.0503	0.0032	0.1322	0.0075	0.0194	0.0003	206	138	128	6.95	123	2.02
10.1	16.5	257	198	1.3	0.0496	0.0031	0.1321	0.0075	0.0194	0.0003	311	135	135	7.21	122	2.05
11.1	19.5	255	206	1.2	0.0512	0.0042	0.1318	0.0102	0.0186	0.0004	255	178	126	9.15	119	2.42
12.1	9.53	139.0	107	1.3	0.0495	0.0031	0.1321	0.0075	0.0193	0.0003	173	135	125	6.76	123	1.83
BS01																
Spot	Pb (ppm)	Th (ppm)	U (ppm)	Th/U	$^{207}\text{Pb}/^{206}\text{Pb}$	$1\sigma$	$^{207}\text{Pb}/^{235}\text{U}$	$1\sigma$	$^{206}\text{Pb}/^{238}\text{U}$	$1\sigma$	$^{207}\text{Pb}/^{206}\text{Pb}$	$1\sigma$	$^{207}\text{Pb}/^{235}\text{U}$	$1\sigma$	$^{206}\text{Pb}/^{238}\text{U}$	$1\sigma$
1.1	16.5	196	145	1.4	0.0502	0.0045	0.1326	0.0096	0.0192	0.0003	205	202	130	10.6	123	2.75
2.1	15.5	243	174	1.4	0.0505	0.0045	0.1326	0.0098	0.0192	0.0003	216	155	129	8.13	122	2.25
3.1	25.8	248	221	1.1	0.0503	0.0043	0.1325	0.0098	0.0191	0.0004	86	163	125	8.05	122	2.28
4.1	13.5	152	124	1.2	0.0495	0.0044	0.1325	0.0095	0.0188	0.0003	195	138	126	7.02	122	2.05
5.1	12.4	143	116	1.2	0.0493	0.0045	0.1316	0.0085	0.0186	0.0003	283	155	135	8.61	119	2.28
6.1	14.4	135	103	1.3	0.0491	0.0046	0.1315	0.0082	0.0185	0.0003	145	205	126	10.6	121	2.73
7.1	11.3	142	105	1.4	0.0649	0.0063	0.1313	0.0082	0.0185	0.0004	368	182	162	13.8	120	3.15
8.1	17.6	234	191	1.2	0.0603	0.0056	0.1315	0.0086	0.0186	0.0004	615	186	152	12.5	121	2.95
9.1	9.45	116.0	95.6	1.2	0.0606	0.0055	0.1355	0.0082	0.0192	0.0003	342	222	138	13.2	123	3.18
10.1	23.2	246	206	1.2	0.0605	0.0055	0.1356	0.0082	0.0192	0.0003	515	155	148	9.58	122	2.45
11.1	20.0	253	214	1.2	0.0508	0.0036	0.1356	0.0081	0.0191	0.0003	231	163	128	8.52	123	2.32
12.1	15.3	182	145	1.3	0.0705	0.0043	0.1354	0.0082	0.0192	0.0003	195	118	175	9.05	123	2.21

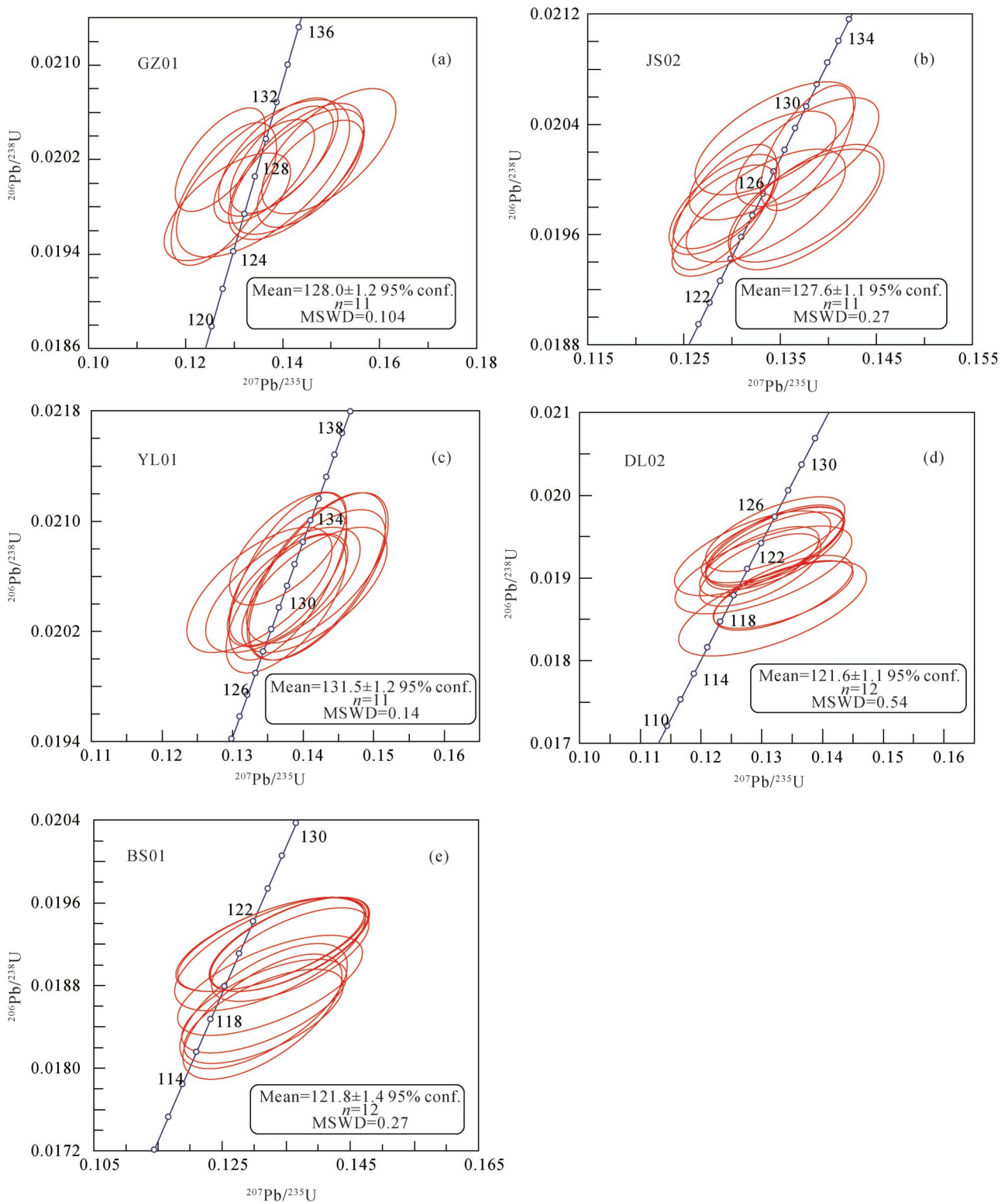


Fig. 2. LA-ICP-MS U-Pb concordia diagrams for the southern WMGL mafic dykes.

YL01 zircon, yielding variable  $\varepsilon_{\text{Hf}}(t)$  values between  $-14.9$  and  $-17.7$  (Table 6; Fig. 8e, f), twostage model ages ( $T_{\text{DM1}}$ ) of 1,402 to 1,500 Ma (Table 6; Fig. 8e, f), and giving initial  $^{176}\text{Hf}/^{177}\text{Hf}$  ratios of 0.282194 to 0.282272. Sixteen spot analyses were obtained for DL02 zircon

samples, yielding variable  $\varepsilon_{\text{Hf}}(t)$  values between  $-28.4$  and  $-30.4$  (Table 6; Fig. 8g, h), one-stage model ages ( $T_{\text{DM1}}$ ) of 1,905 to 1,988 Ma (Table 6; Fig. 8g, h), and initial  $^{176}\text{Hf}/^{177}\text{Hf}$  ratios of 0.281838 to 0.281895. Seventeen spot analyses were obtained for the zircon from

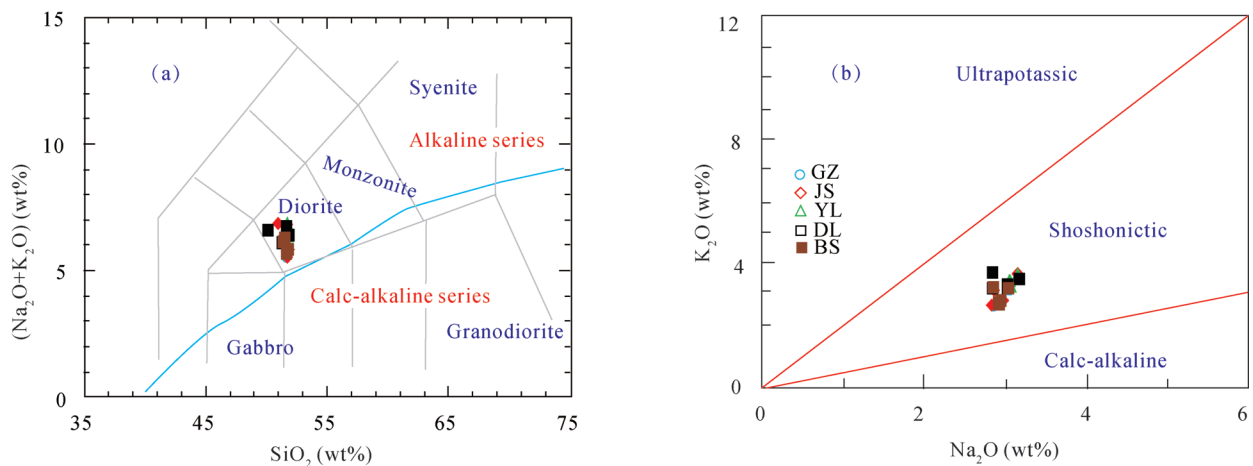


Fig. 3. Plots of total alkali vs. silica (TAS).

(a)  $\text{Na}_2\text{O}$  vs.  $\text{K}_2\text{O}$  for the mafic dykes studied; (b) plots for the mafic dykes within the WMGL study areas. All major element data have been recalculated to 100% on an anhydrous basis (Middlemost, 1994; Le Maitre, 2002).

**Table 2 Whole rock major element (wt%) composition results for the mafic dykes studied**

Sample No.	GZ1	GZ2	GZ4	GZ6	GZ8	JS1	JS3	JS4	JS6	JS9	YL1	YL2	YL4	YL6
Rock type	Dolerite													
Region	Guzhang					Jishou				Yuanling				
$\text{SiO}_2$	51.65	51.43	51.54	51.65	51.55	51.28	51.76	51.66	51.65	50.88	51.66	51.55	51.67	51.36
$\text{TiO}_2$	1.12	1.23	1.03	1.15	1.14	1.26	1.07	1.13	1.28	1.28	1.28	1.33	1.25	1.25
$\text{Al}_2\text{O}_3$	15.85	16.18	16.34	15.82	15.96	16.35	15.93	15.85	16.37	16.54	16.24	16.15	16.19	16.09
$\text{Fe}_2\text{O}_3$	8.85	7.82	7.42	8.96	8.75	7.87	8.81	8.95	8.05	8.97	9.07	9.15	9.66	9.04
MnO	0.15	0.16	0.16	0.15	0.18	0.18	0.16	0.16	0.16	0.15	0.16	0.15	0.16	0.15
MgO	5.86	5.78	5.61	6.63	6.15	5.85	6.41	6.55	5.22	5.19	5.15	5.35	5.25	5.18
CaO	7.85	7.76	7.63	7.65	7.43	7.83	7.43	7.62	6.94	7.02	7.06	7.18	7.09	7.06
$\text{Na}_2\text{O}$	2.95	2.86	3.05	2.86	3.06	2.86	2.98	2.83	3.15	3.15	3.15	3.05	3.06	3.05
$\text{K}_2\text{O}$	2.74	3.16	3.16	2.62	3.12	3.14	2.81	2.66	3.64	3.68	3.65	3.43	3.43	3.35
$\text{P}_2\text{O}_5$	0.52	1.24	0.93	0.51	0.46	1.26	0.44	0.45	0.73	0.72	0.67	0.71	0.66	0.67
LOI	1.68	1.73	2.42	1.33	1.66	1.35	1.58	1.46	2.36	1.85	1.38	1.43	1.21	2.25
Total	99.22	99.35	99.29	99.33	99.46	99.23	98.31	99.32	99.55	99.43	99.47	99.48	99.63	99.45
Mg <sup>#</sup>	57	59	60	59	58	60	59	59	56	53	53	54	52	53
T (°C)	821	811	812	817	810	805	823	821	808	803	801	799	804	801

YL7	DL2	DL3	DL5	DL6	DL10	BS1	BS3	BS5	BS7	BS8
Dolerite	Dolerite	Dolerite	Dolerite	Dolerite	Dolerite	Dolerite	Dolerite	Dolerite	Dolerite	Dolerite
Region	Donglan			Baise		Yixian				
$\text{SiO}_2$	51.68	51.86	51.65	50.14	51.48	51.26	51.52	51.38	51.66	51.76
$\text{TiO}_2$	1.26	1.28	1.26	1.29	0.95	1.27	0.96	1.25	1.08	1.08
$\text{Al}_2\text{O}_3$	16.06	16.06	15.95	15.46	16.35	16.35	16.36	16.24	15.83	15.95
$\text{Fe}_2\text{O}_3$	8.95	8.93	9.46	9.64	7.34	7.85	7.41	7.83	8.83	8.83
MnO	0.16	0.15	0.15	0.13	0.16	0.18	0.15	0.16	0.16	0.15
MgO	5.06	5.43	5.56	6.15	5.58	5.83	5.56	5.76	5.95	6.45
CaO	6.88	7.05	7.25	7.94	7.65	7.76	7.63	7.76	7.83	7.43
$\text{Na}_2\text{O}$	3.07	3.04	3.19	2.85	3.04	2.85	3.05	2.87	2.93	2.96
$\text{K}_2\text{O}$	3.26	3.27	3.46	3.67	3.15	3.15	3.17	3.18	2.72	2.78
$\text{P}_2\text{O}_5$	0.69	0.72	0.69	0.66	0.95	1.25	0.95	1.23	0.49	0.54
LOI	2.32	1.58	0.78	1.45	1.56	1.58	2.45	1.66	1.76	1.55
Total	99.39	99.37	99.40	99.38	98.21	99.33	99.21	99.32	99.24	99.48
Mg <sup>#</sup>	53	55	54	56	60	60	60	59	57	59
T (°C)	803	801	796	787	813	804	813	806	818	825

BS01, that yield variable  $\varepsilon_{\text{Hf}}(t)$  values between  $-27.6$  and  $-30.3$  (Table 6; Fig. 8i, j), one-stage model ages from 1,917 to 2,007 Ma (Table 6; Fig. 8i, j), and initial  $^{176}\text{Hf}/^{177}\text{Hf}$  ratios from 0.281843 to 0.281921.

## 5 Discussions

### 5.1 Fractional crystallization

The observed  $\text{Mg}^{\#}$  (52–60), for the mafic dykes from

the WMGL study areas is inconsistent with significant crystal fractionation. However, these dolerites contain lower Cr (almost all less than 250 ppm except DL3 and DL5) and Ni (6.7–167 ppm; Table 3), implying that they were derived by fractional crystallization. Further support for this are given in the  $\text{MgO}$  vs.  $(^{87}\text{Sr}/^{86}\text{Sr})_i$ ,  $\varepsilon_{\text{Nd}}(t)$  and  $(^{206}\text{Pb}/^{204}\text{Pb})_i$  correlative plots (Fig. 9), and the correlation between  $\text{MgO}$  content and  $\text{SiO}_2$ ,  $\text{CaO}$ ,  $\text{TiO}_2$ ,  $\text{Na}_2\text{O}$ ,  $\text{Al}_2\text{O}_3$ ,  $\text{K}_2\text{O}$ ,  $\text{Fe}_2\text{O}_3$ ,  $\text{P}_2\text{O}_5$  (Fig. 4), Sr and Zr (not shown) favors

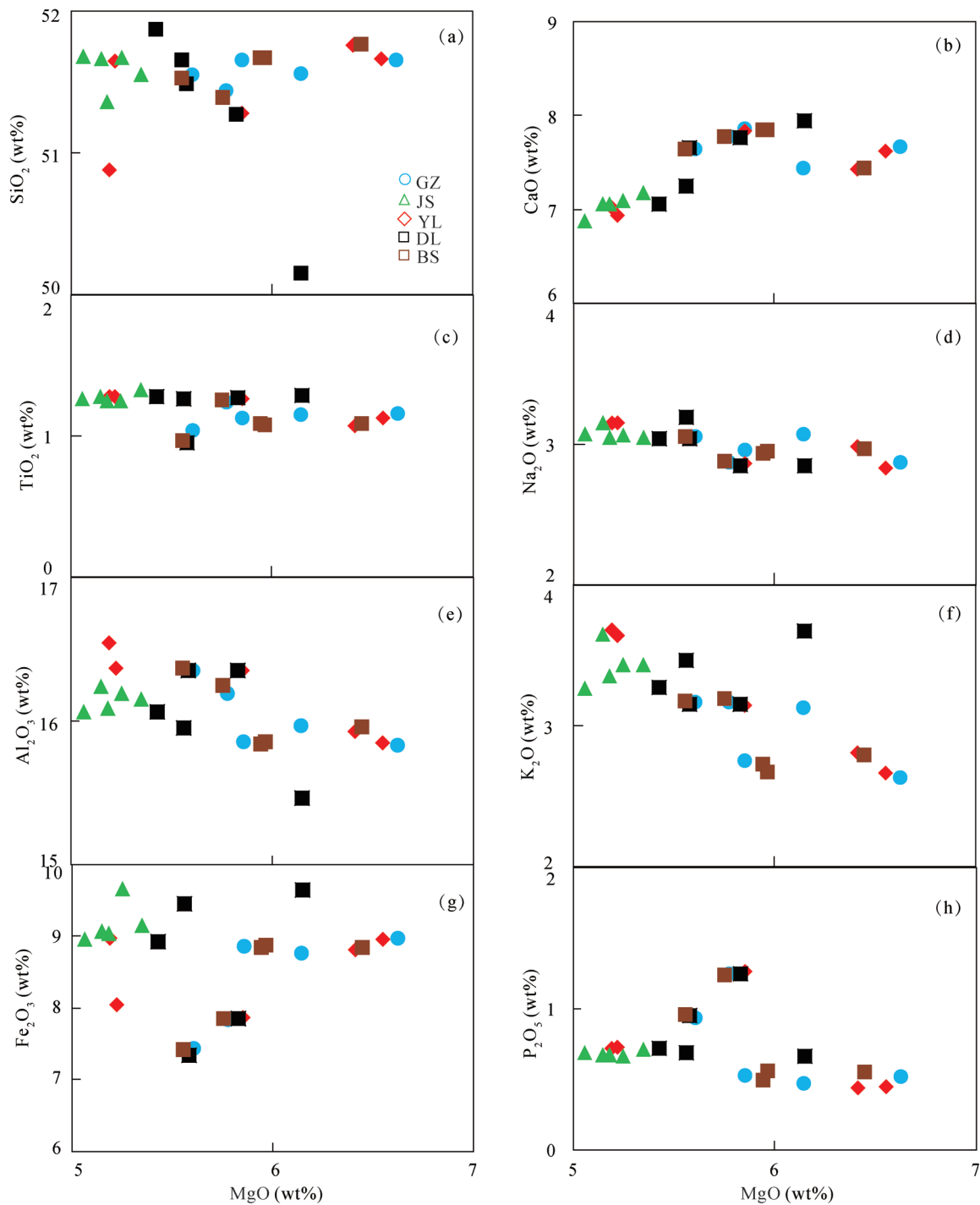


Fig. 4.  $\text{SiO}_2$ ,  $\text{CaO}$ ,  $\text{TiO}_2$ ,  $\text{Na}_2\text{O}$ ,  $\text{Al}_2\text{O}_3$ ,  $\text{K}_2\text{O}$ ,  $\text{Fe}_2\text{O}_3$ , and  $\text{P}_2\text{O}_5$  vs.  $\text{MgO}$  plots for the WMGL mafic dykes.

fractionation of olivine, clinopyroxene, plagioclase, Ti-bearing phases (rutile, ilmenite, titanite, etc.) in the genesis of the WMGL mafic magmas. The separation of plagioclase, Ti-bearing oxides and apatite is also supported by the negative Eu, Nb, Ta, Ti anomalies observed in the chondrite-normalized REE pattern and primitive mantle-normalized spider diagrams (Fig. 5a, b), and in plots of Sr vs. Ba and Rb (not shown). Clearly, the WMGL mafic dykes as studied exhibit decreasing Zr with

increasing  $\text{SiO}_2$  (not shown) indicating that zircon was saturated in the magma and is also controlled by fractional crystallization (Li et al., 2007).

### 5.2 Crustal assimilation

Crustal contamination might cause a significant depletion in Nb-Ta and enriched Sr-Nd isotopic signatures in basaltic rocks. The WMGL dolerites as studied are characterized by negative Nb-Ta anomalies (Table 3; Fig.

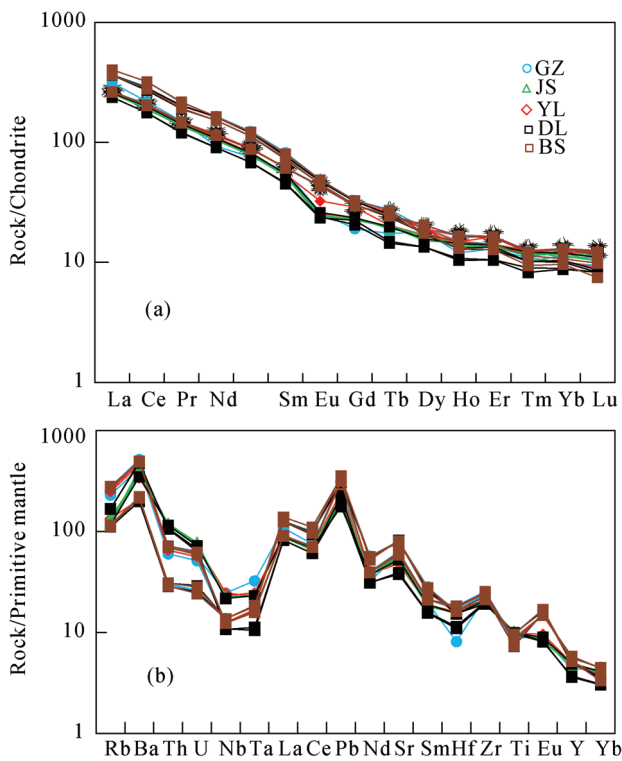


Fig. 5. Chondrite-normalized REE diagrams and primitive mantle-normalized element distribution spider-diagrams for the mafic dykes studied. The normalization values are from Sun and McDonough (1989).

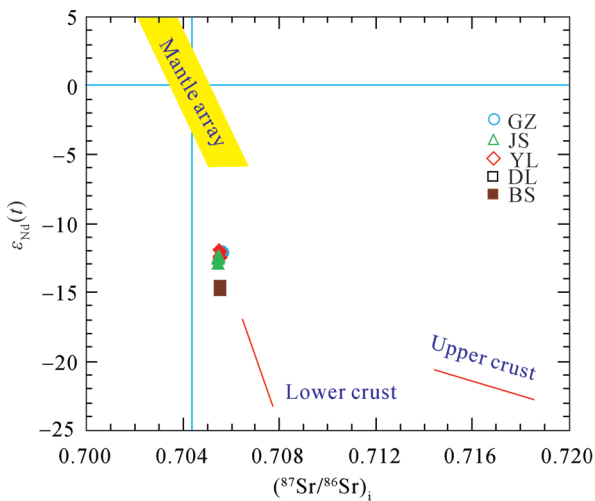


Fig. 6. Initial  $^{87}\text{Sr}/^{86}\text{Sr}$  vs.  $\varepsilon_{\text{Nd}}(t)$  diagram for the mafic dykes studied.

5b), high Sr isotopic compositions (0.7055–0.7057) and negative  $\varepsilon_{\text{Nd}}(t)$  (–11.9 to –14.8) (Table 4; Fig. 5); these data might imply a crustal component in the magma genesis of the dolerites. Further support for this is given in their determined low Nb/U (5.4–19; Table 3) (cf. Nb/U = 9.0–21 for crust, and Nb/U = 47 for primitive mantle), and Ta/La ratios (0.01–0.02; Table 3) (cf. Ta/La = 0.06 for primitive mantle). Nevertheless, crustal assimilation

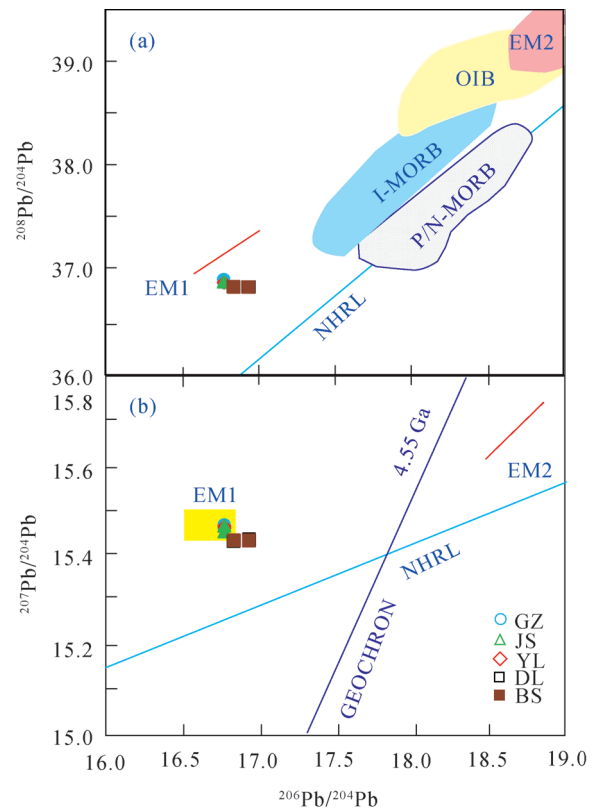


Fig. 7.  $^{208}\text{Pb}/^{204}\text{Pb}$  and  $^{207}\text{Pb}/^{204}\text{Pb}$  vs.  $^{206}\text{Pb}/^{204}\text{Pb}$  diagrams for the mafic dykes studied.

Field for I-MORB (Indian MORB) and P & N-MORB (Pacific and North Atlantic MORB), OIB, NHRL and 4.55 Ga geochron are after Barry and Kent (1998), Zou et al. (2000), and Hart (1984), respectively.

would result in a positive correlation between MgO and  $\varepsilon_{\text{Nd}}(t)$  values, and negative correlation between MgO and initial  $^{87}\text{Sr}/^{86}\text{Sr}$  ratios; features that are not observed in these rocks (Table 4; Fig. 9a, b). Moreover, the dykes studied are characterized by relatively lower Nb (7.65–17.5 ppm), Th (2.43–10.2 ppm), and U (0.53–1.64 ppm) (Table 3) compared to upper crust (e.g., Nb = 25 ppm, Th = 10.5 ppm, U = 2.7 ppm, Rudnick and Fountain, 1995), suggesting that crustal contamination was likely negligible in the WMGL dolerites. This conclusion is further supported in the lack of inherited zircon component within the studied mafic dyke samples.

### 5.3 Source and partial melting

The high initial  $^{87}\text{Sr}/^{86}\text{Sr}$  ratios (0.7055–0.7057), negative  $\varepsilon_{\text{Nd}}(t)$  (–11.9 to –14.8), and negative zircon  $\varepsilon_{\text{Hf}}(t)$  values (–14.9 to –30.4) for the studied dolerite samples (Tables 4, 6) are all consistent with their derivation from an enriched lithospheric mantle source, rather than from an asthenospheric mantle source, with a depleted Sr–Nd–Hf isotopic composition, such as mid–ocean ridge basalt. Such an enriched mantle source is found beneath the study area (Liu et al., 2008a, b, 2009). This hypothesis is further supported in the EM1-like Pb isotopic compositions ( $^{206}\text{Pb}/^{204}\text{Pb}$ )<sub>i</sub> = 16.77–16.94, ( $^{207}\text{Pb}/^{204}\text{Pb}$ )<sub>i</sub> = 15.43–15.47,

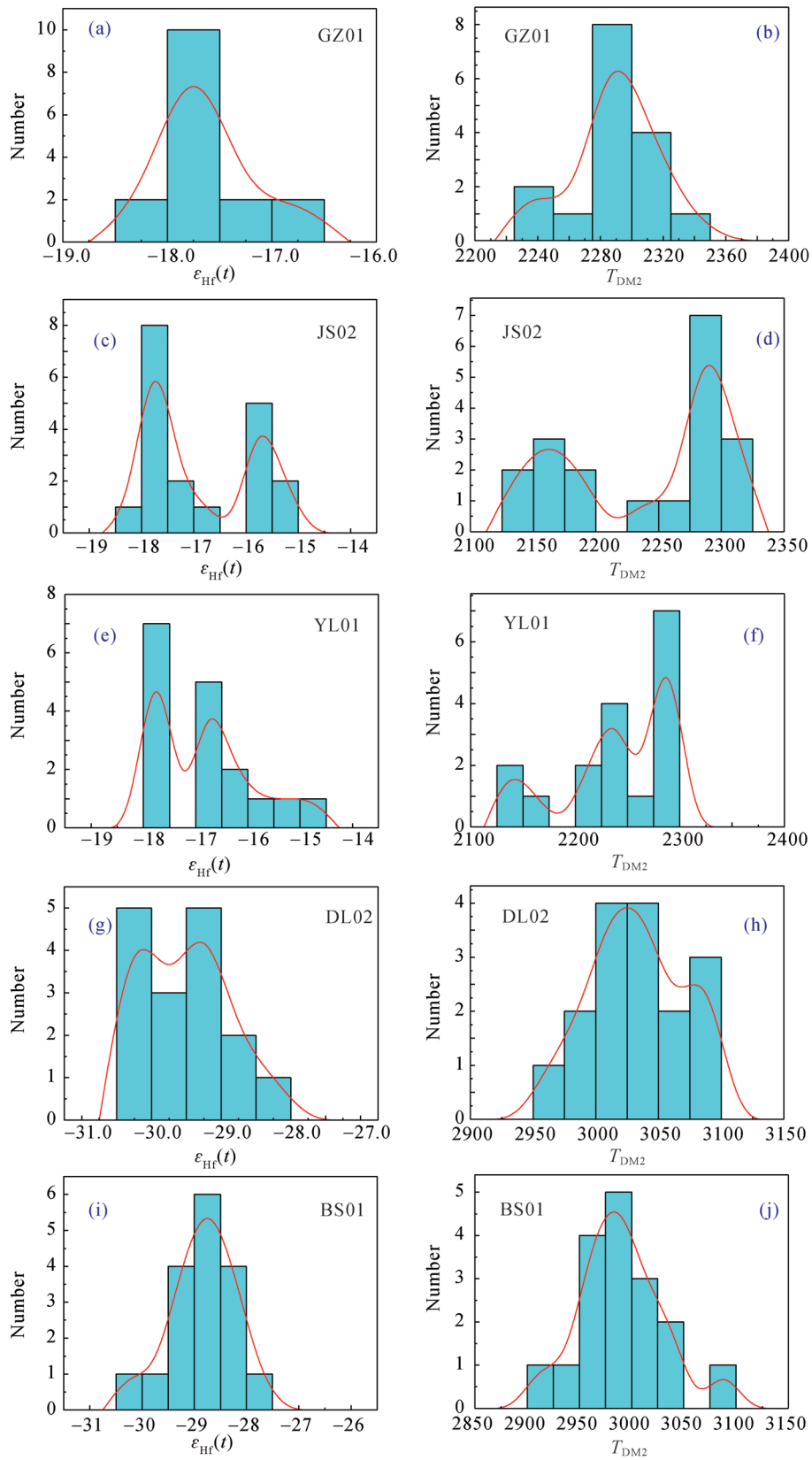


Fig. 8. Histograms of  $T_{DM2}$  for the zircons from the mafic dykes studied.

**Table 3 Trace element analysis results (ppm) of the mafic dykes**

Sample No.	GZ1	GZ2	GZ4	GZ6	GZ8	JS1	JS3	JS4	JS6	JS9	YL1	YL2	YL4	YL6	YL7
Rock type	Dolerite														
Region	Guzhang					Jishou					Yuanling				
V	227	158	173	188	195	143	218	196	138	136	142	147	146	143	141
Cr	236	65.4	66.2	227	9.65	63.4	243	234	142	136	148	154	156	162	145
Co	39.3	24.2	24.7	36.2	2.57	23.4	36.5	35.7	22.2	21.3	22.8	23.8	23.5	23.2	22.8
Ni	80.6	50.5	48.8	78.8	6.65	48.5	78.6	76.4	43.6	43.2	48.8	50.4	50.9	61.5	48.4
Ga	24.3	23.2	21.5	21.8	21.6	22.2	23.1	22.7	17.5	17.3	16.5	16.8	17.2	16.5	17.4
Rb	175	71.5	73.4	146	159	85.6	166	157	84.3	84.5	86.8	81.2	80.5	76.6	76.4
Sr	1332	1694	1742	1132	1275	1648	1228	1156	1043	1015	1154	1215	1168	1106	1084
Y	25.2	23.5	23.6	25.5	19.8	22.4	25.6	25.8	22.8	21.8	21.6	22.5	22.4	21.6	22.6
Zr	285	254	254	264	248	236	278	274	232	225	221	216	225	218	216
Nb	8.78	9.82	9.75	8.86	17.5	9.76	8.76	8.95	17.5	16.5	16.3	16.3	16.2	15.6	15.6
Ba	3618	1482	1526	2984	3256	1443	3422	3234	2416	2376	2546	2648	2483	2915	2438
Hf	5.66	4.95	5.04	5.25	2.51	4.69	5.53	5.44	4.93	4.95	4.81	4.76	4.83	4.81	4.84
Ta	0.67	0.75	0.75	0.66	1.33	0.75	0.67	0.69	0.94	1.01	0.93	0.95	0.94	0.94	0.94
Pb	23.6	24.3	25.3	21.4	21.3	22.5	22.2	21.8	13.2	17.5	15.1	14.6	13.4	15.9	12.4
Th	6.13	2.53	2.58	5.11	5.56	2.44	5.86	5.53	9.79	9.96	9.81	9.91	10.1	10.1	10.2
U	1.34	0.55	0.55	1.08	1.19	0.51	1.25	1.18	1.53	1.56	1.53	1.52	1.56	1.64	1.63
La	62.5	95.4	86.7	61.5	74.2	85.4	62.5	61.8	63.2	62.7	60.5	60.3	60.6	60.8	60.5
Ce	128	196	178	126	134	172	126	127	125	124	116	118	120	123	123
Pr	13.9	20.3	18.3	13.9	14.3	19.1	14.1	14.1	13.6	14.1	12.9	13.3	13.4	13.6	13.6
Nd	54.3	77.2	71.1	54.3	43.4	75.6	54.4	54.6	51.2	51.4	48.5	50.1	50.1	50.2	50.2
Sm	9.43	12.6	11.3	9.41	8.81	11.6	9.39	9.43	8.34	8.33	8.01	8.15	8.14	8.16	8.04
Eu	2.53	2.84	2.60	2.51	1.51	2.74	2.49	2.51	1.88	1.82	1.37	1.41	1.42	1.43	1.45
Gd	6.03	6.76	6.20	6.11	3.91	5.63	5.93	5.83	5.94	5.88	4.84	4.63	4.72	4.71	4.62
Tb	0.96	1.03	0.92	0.95	0.65	0.96	0.94	0.94	0.76	0.74	0.71	0.75	0.74	0.75	0.74
Dy	4.05	4.02	3.93	4.03	3.62	4.84	4.83	4.81	4.31	4.31	4.33	4.27	4.23	3.84	4.03
Ho	0.96	0.85	0.75	0.94	0.68	0.76	0.84	0.95	0.83	0.81	0.77	0.79	0.81	0.82	0.82
Er	2.73	2.35	2.10	2.71	2.15	2.22	2.71	2.72	2.33	2.35	2.23	2.29	2.21	2.31	2.28
Tm	0.32	0.32	0.28	0.31	0.31	0.26	0.31	0.32	0.32	0.31	0.26	0.31	0.29	0.30	0.29
Yb	2.22	1.85	1.69	2.21	2.12	1.74	2.19	2.21	1.98	2.04	1.93	1.94	2.03	1.96	2.01
Lu	0.32	0.28	0.24	0.31	0.31	0.23	0.31	0.32	0.29	0.31	0.26	0.26	0.26	0.31	0.29
Eu/Eu*	0.96	0.85	0.86	0.95	0.68	0.88	0.94	0.95	0.64	0.66	0.62	0.64	0.64	0.65	0.67
(La/Yb) <sub>N</sub>	20.2	37.0	36.8	20.0	25.1	35.2	20.5	20.1	22.9	22.1	22.5	22.3	21.4	22.3	21.6

DL2	DL3	DL5	DL6	DL10	BS1	BS3	BS5	BS7	BS8
Dolerite									
Donglan					Baise		Yixian		
143	152	151	168	144	176	167	221	225	223
148	465	479	66.8	63.5	65.8	65.6	243	245	244
23.1	33.2	32.8	25.4	23.2	24.6	24.3	38.4	36.8	38.3
49.6	165	167	49.3	48.5	48.8	48.9	78.6	78.8	78.5
17.2	14.8	14.4	21.6	21.8	21.6	22.8	23.6	23.4	23.7
73.8	106	107	73.4	70.6	73.8	71.4	172	178	174
1114	798	826	1725	1664	1708	1682	1312	1238	1294
22.2	16.8	16.4	23.5	22.6	23.6	23.5	25.4	26.4	25.3
215	217	225	256	231	256	238	277	283	269
15.5	7.75	7.65	9.72	9.75	9.75	9.74	8.81	8.82	8.82
2445	3418	3343	1526	1395	1544	1512	3491	3428	3474
4.76	3.39	3.53	5.03	4.72	5.04	5.01	5.63	5.46	5.62
0.95	0.43	0.46	0.75	0.74	0.74	0.76	0.66	0.67	0.65
12.6	13.4	16.1	25.3	21.7	25.2	24.4	22.4	23.3	22.8
9.82	9.02	9.15	2.61	2.43	2.63	2.46	6.11	5.92	6.12
1.52	1.34	1.41	0.61	0.53	0.59	0.51	1.28	1.24	1.31
60.9	56.3	56.4	86.2	86.6	86.4	95.4	62.8	62.7	62.2
122	108	108	166	174	171	196	126	125	124
13.5	11.5	11.4	18.1	19.3	18.3	20.6	14.1	13.8	14.1
50.3	42.3	42.1	71.1	76.2	71.2	76.3	53.6	53.6	53.3
8.41	6.91	7.02	11.1	11.8	11.0	12.3	9.41	9.34	9.43
1.51	1.36	1.39	2.61	2.74	2.61	2.83	2.51	2.49	2.51
4.83	4.61	4.23	6.21	6.62	6.21	6.74	6.13	6.08	6.09
0.74	0.56	0.54	0.89	0.94	0.91	1.01	0.93	0.92	0.93
4.01	3.41	3.41	4.43	4.36	4.44	4.43	5.21	5.18	5.21
0.81	0.61	0.59	0.73	0.74	0.74	0.84	0.93	0.94	0.93
2.31	1.74	1.73	2.11	2.23	2.11	2.34	2.72	2.71	2.66
0.31	0.23	0.21	0.26	0.26	0.24	0.29	0.31	0.31	0.31
2.03	1.51	1.49	1.71	1.76	1.64	1.82	2.21	2.19	2.21
0.28	0.21	0.21	0.21	0.22	0.19	0.25	0.29	0.30	0.31
0.66	0.69	0.72	0.88	0.87	0.88	0.86	0.95	0.95	0.95
21.5	26.8	27.2	36.2	35.3	37.8	37.6	20.4	20.5	20.2

**Table 4 Sr–Nd isotopic ratios for representative mafic dykes**

Sample	Age (Ma)	Rb (ppm)	Sr (ppm)	$^{87}\text{Rb}/^{86}\text{Sr}$	$^{87}\text{Sr}/^{86}\text{Sr}$	$\pm 2\sigma$	Sm (ppm)	Nd (ppm)	$^{147}\text{Sm}/^{144}\text{Nd}$	$^{143}\text{Nd}/^{144}\text{Nd}$	$\pm 2\sigma$	$(^{87}\text{Sr}/^{86}\text{Sr})_i$	$(^{143}\text{Nd}/^{144}\text{Nd})_i$	$\epsilon_{\text{Nd}} (t)$
GZ1	128	33.6	348	0.2796	0.706203	12	7.45	31.8	0.1416	0.511969	9	0.511945	0.511850	-12.2
GZ2	128	25.2	265	0.2754	0.706182	13	7.56	34.2	0.1336	0.511965	10	0.511940	0.511853	-12.1
GZ4	128	36.4	418	0.2522	0.706108	14	7.95	35.9	0.1339	0.511964	10	0.511937	0.511852	-12.1
GZ6	128	35.5	386	0.2663	0.706133	13	7.83	35.3	0.1341	0.511963	9	0.511938	0.511851	-12.1
GZ8	128	46.6	561	0.2405	0.706115	14	8.42	38.7	0.1315	0.511955	8	0.511929	0.511845	-12.3
JS1	128	81.6	643	0.3675	0.706172	11	8.53	39.1	0.1319	0.511975	12	0.511955	0.511865	-11.9
JS3	128	79.3	615	0.3734	0.706192	12	7.89	35.4	0.1347	0.511945	10	0.511922	0.511833	-12.5
JS4	128	79.4	609	0.3775	0.706198	13	7.87	35.2	0.1352	0.511954	10	0.511929	0.511841	-12.3
JS6	128	69.4	567	0.3544	0.706224	12	7.17	32.4	0.1338	0.511969	10	0.511946	0.511857	-12.0
JS9	128	72.5	584	0.3595	0.706235	13	7.25	32.6	0.1344	0.511945	9	0.511920	0.511829	-12.5
YL1	131.5	66.2	528	0.3630	0.706172	12	7.75	34.9	0.1342	0.511951	9	0.511928	0.511836	-12.4
YL2	131.5	67.6	549	0.3565	0.706165	14	7.87	35.3	0.1348	0.511949	9	0.511922	0.511833	-12.4
YL4	131.5	69.1	563	0.3554	0.706161	13	7.69	33.7	0.1379	0.511951	8	0.511926	0.511832	-12.4
YL6	131.5	74.5	594	0.3632	0.706164	12	8.16	36.4	0.1355	0.511945	10	0.511922	0.511828	-12.5
YL7	131.5	82.3	654	0.3644	0.706166	14	9.75	41.6	0.1417	0.511936	9	0.511908	0.511823	-12.8
DL2	121.6	27.3	268	0.2950	0.706105	12	4.53	18.2	0.1505	0.511845	9	0.511819	0.511725	-14.8
DL3	121.6	32.4	316	0.2969	0.706106	10	4.56	18.2	0.1515	0.511847	9	0.511825	0.511727	-14.7
DL5	121.6	35.3	338	0.3024	0.706114	14	6.05	23.6	0.1550	0.511851	7	0.511820	0.511728	-14.7
DL6	121.6	38.2	373	0.2965	0.706108	13	8.21	32.6	0.1522	0.511845	10	0.511817	0.511724	-14.8
DL10	121.6	41.6	398	0.3027	0.706117	12	9.64	38.5	0.1514	0.511849	6	0.511823	0.511728	-14.7
BS1	121.8	23.5	232	0.2933	0.706105	11	22.3	88.4	0.1525	0.511851	10	0.511827	0.511729	-14.7
BS3	121.8	24.6	243	0.2931	0.706103	14	23.5	93.2	0.1524	0.511846	8	0.511816	0.511725	-14.8
BS5	121.8	26.2	257	0.2952	0.706105	13	24.6	96.4	0.1543	0.511849	9	0.511821	0.511726	-14.7
BS7	121.8	34.3	336	0.2956	0.706108	12	32.4	126	0.1554	0.511846	10	0.511820	0.511722	-14.8
BS8	121.8	35.4	345	0.2971	0.706112	12	29.2	113	0.1562	0.511854	9	0.511827	0.511724	-14.6

**Table 5 Pb isotopic ratios for representative mafic dykes**

Sample	Age (Ma)	$^{206}\text{Pb}/^{204}\text{Pb}$	$^{207}\text{Pb}/^{204}\text{Pb}$	$^{208}\text{Pb}/^{204}\text{Pb}$	U (ppm)	Pb (ppm)	Th (ppm)	$^{238}\text{U}/^{204}\text{Pb}$	$^{235}\text{U}/^{204}\text{Pb}$	$^{232}\text{Th}/^{204}\text{Pb}$	$(^{206}\text{Pb}/^{204}\text{Pb})_i$	$(^{207}\text{Pb}/^{204}\text{Pb})_i$	$(^{208}\text{Pb}/^{204}\text{Pb})_i$
GZ1	128	16.815	15.464	36.984	1.65	48.2	8.24	2.1	0.0151	10.7	16.773	15.462	36.916
GZ2	128	16.869	15.469	36.968	1.66	21.8	4.65	4.6	0.0336	13.4	16.776	15.464	36.883
GZ4	128	16.865	15.468	36.973	1.58	21.4	4.64	4.5	0.0325	13.6	16.775	15.464	36.887
GZ6	128	16.816	15.467	36.932	1.24	37.5	4.16	2.0	0.0146	7.0	16.776	15.465	36.888
GZ8	128	16.818	15.471	36.933	1.32	36.4	4.07	2.2	0.0160	7.0	16.774	15.469	36.889
JS1	128	16.822	15.468	36.938	1.26	33.5	4.13	2.3	0.0166	7.7	16.776	15.466	36.889
JS3	128	16.852	15.469	37.139	1.17	19.1	12.2	3.7	0.0271	40.2	16.777	15.465	36.884
JS4	128	16.857	15.468	37.135	1.28	18.7	11.6	4.2	0.0302	39.0	16.774	15.464	36.888
JS6	128	16.931	15.468	37.122	2.05	16.4	9.84	7.6	0.0552	37.8	16.779	15.461	36.883
JS9	128	16.836	15.469	37.026	2.17	44.3	15.6	3.0	0.0216	22.1	16.775	15.466	36.882
YL1	131.5	16.838	15.471	37.028	2.26	45.7	15.8	3.0	0.0218	21.7	16.776	15.468	36.886
YL2	131.5	16.835	15.469	37.021	2.18	44.5	13.4	3.0	0.0216	18.9	16.774	15.466	36.898
YL4	131.5	16.818	15.467	36.968	1.54	45.7	8.35	2.0	0.0148	11.5	16.776	15.465	36.893
YL6	131.5	16.883	15.458	36.988	1.65	19.3	4.64	5.2	0.0377	15.1	16.776	15.453	36.889
YL7	131.5	16.814	15.456	36.956	1.48	44.3	8.16	2.0	0.0147	11.6	16.775	15.454	36.886
DL2	121.6	16.997	15.438	36.956	2.32	44.5	13.2	3.2	0.0233	18.9	16.936	15.435	36.842
DL3	121.6	17.013	15.439	36.958	2.54	38.3	11.2	4.1	0.0297	18.6	16.935	15.435	36.845
DL5	121.6	17.031	15.442	37.003	2.34	29.3	12.3	4.9	0.0358	26.8	16.937	15.437	36.841
DL6	121.6	16.904	15.435	36.976	0.95	16.2	5.46	3.6	0.0262	21.5	16.835	15.432	36.846
DL10	121.6	16.987	15.437	37.113	0.78	20.3	13.1	2.4	0.0172	41.2	16.938	15.435	36.844
BS1	121.8	16.996	15.438	36.921	1.21	26.2	4.78	2.8	0.0207	11.6	16.937	15.435	36.845
BS3	121.8	17.006	15.436	36.997	3.45	57.8	23.3	3.7	0.0267	25.7	16.936	15.433	36.842
BS5	121.8	16.911	15.437	36.986	3.38	55.4	20.5	3.8	0.0277	23.9	16.838	15.433	36.842
BS7	121.8	16.903	15.437	36.008	3.66	64.6	27.2	3.5	0.0253	26.8	16.836	15.434	36.846
BS8	121.8	16.905	15.439	36.026	3.56	66.3	28.5	3.3	0.0240	27.4	16.837	15.436	36.847

and  $(^{208}\text{Pb}/^{204}\text{Pb})_i = 36.84\text{--}36.92$  (Table 5; Fig. 7a, b) of the mafic rocks. Also, the investigated dolerites have La/Sm and Sm/Yb (Table 3; Fig. 10a, b) that are consistent with magmas generated by relatively low to moderate degree partial melting (1.0%–10%) of a garnet lherzolite source, which is also supported by their high Ti/Y (192–726; Table 2, 3; Johnson, 1998).

#### 5.4 Origin of the studied WMGL mafic dykes

South China is situated on the eastern margin of Eurasia

and borders the western Pacific Ocean. Tectonically, this block comprises the Cathaysian and the Yangtze terranes, having been formed through their collision and collage in Early Neoproterozoic (Fan et al., 2003; Mao et al., 2014; Zhang and Zhang, 2013). Mesozoic igneous rocks are widely developed across South China. Although some studies have focused on these rocks, it remains controversial about their origins (i.e., subduction of the Mesozoic Paleo-Pacific Plate, deep mantle heat sources in the Asian continent, orogeny due to the collision between

Yangtze Block and Cathaysian Block) (Uyeda and Miyashiro, 1974; Zhang, 1986; Charvet et al., 1996; Chen and Jahn, 1998; Fan et al., 2003; Wang et al., 2005; Zhou et al., 2006; Li et al., 2007, Li and Li, 2007; Zhang et al., 2012). Mesozoic was a period of strong tectonic movement and transition in South China (e.g., EW-trending Tethys tectonic domain in the Indosinian, followed by the littoral Pacific tectonic domain during the Early Yanshanian; Ren, 1990; Zhao et al., 2004; Dong et al., 2008; Dong et al., 2010; Zhang et al., 2012). In

general, the genetic model for the Mesozoic mafic dykes with EM1-like source may come from partial melting of the assimilation and fractional crystallization in the lower crust (Liu, 2004; Liu et al., 2008a, b, 2009, 2017, 2018; Li et al., 2004; Long, 2017). Based on the above discussion, though minor fractionation of olivine, clinopyroxene, plagioclase, and Ti-bearing phases occurred during magma ascent, negligible crustal contamination precluded this model. Furthermore, as the mantle portion between 410 km and 660 km discontinuities, mantle transition zone

**Table 6** In-situ Hf isotopic results for the mafic dykes

GZ01								
Spot	$^{176}\text{Yb}/^{177}\text{Hf}$	$^{176}\text{Lu}/^{177}\text{Hf}$	$^{176}\text{Hf}/^{177}\text{Hf}$	$2\sigma$	$\epsilon_{\text{Hf}}(t)$	$T_{\text{DM1}}$ (Ma)	$T_{\text{DM2}}$ (Ma)	$f_{\text{Lu/Hf}}$
1	0.053867	0.000894	0.282187	0.000016	-18.0	1499	2315	-0.97
2	0.050965	0.000857	0.282225	0.000015	-16.6	1444	2231	-0.97
3	0.054884	0.000885	0.282176	0.000015	-18.4	1513	2340	-0.97
4	0.097237	0.001785	0.282195	0.000016	-17.8	1523	2302	-0.95
5	0.078921	0.001339	0.282195	0.000016	-17.7	1505	2300	-0.96
6	0.062114	0.001092	0.282196	0.000015	-17.7	1494	2296	-0.97
7	0.078105	0.001243	0.282195	0.000014	-17.7	1501	2299	-0.96
8	0.096913	0.001515	0.282207	0.000015	-17.3	1495	2274	-0.95
9	0.043238	0.001144	0.282196	0.000016	-17.7	1496	2296	-0.97
10	0.050658	0.000793	0.282195	0.000015	-17.7	1483	2297	-0.98
11	0.036065	0.0008073	0.282198	0.000015	-18.2	1828	2324	-0.96
12	0.052413	0.001386	0.282205	0.000014	-17.4	1493	2278	-0.96
13	0.038515	0.000645	0.282191	0.000015	-17.8	1483	2305	-0.98
14	0.055417	0.000896	0.282198	0.000016	-17.6	1483	2291	-0.97
15	0.065084	0.001054	0.282196	0.000016	-17.7	1492	2296	-0.97
16	0.011106	0.001912	0.282226	0.000014	-16.7	1484	2234	-0.94
JS02								
Spot	$^{176}\text{Yb}/^{177}\text{Hf}$	$^{176}\text{Lu}/^{177}\text{Hf}$	$^{176}\text{Hf}/^{177}\text{Hf}$	$2\sigma$	$\epsilon_{\text{Hf}}(t)$	$T_{\text{DM1}}$ (Ma)	$T_{\text{DM2}}$ (Ma)	$f_{\text{Lu/Hf}}$
1	0.024488	0.000815	0.282186	0.000015	-18.0	1497	2317	-0.98
2	0.022708	0.000748	0.282194	0.000016	-17.7	1483	2299	-0.98
3	0.019306	0.000625	0.282183	0.000015	-18.1	1494	2323	-0.98
4	0.022119	0.000725	0.282194	0.000015	-17.7	1482	2299	-0.98
5	0.018676	0.000617	0.282192	0.000016	-17.8	1481	2303	-0.98
6	0.022156	0.000748	0.282196	0.000015	-17.6	1480	2295	-0.98
7	0.025185	0.000845	0.282207	0.000015	-17.3	1469	2271	-0.97
8	0.024258	0.000826	0.282217	0.000015	-16.9	1454	2248	-0.98
9	0.026046	0.000894	0.282265	0.000014	-15.2	1390	2142	-0.97
10	0.022046	0.000754	0.282256	0.000015	-15.5	1397	2161	-0.98
11	0.017582	0.000621	0.282248	0.000015	-15.8	1404	2178	-0.98
12	0.023758	0.000826	0.282245	0.000016	-15.9	1415	2186	-0.98
13	0.017026	0.000596	0.282254	0.000015	-15.6	1394	2165	-0.98
14	0.020711	0.000736	0.282195	0.000014	-17.7	1481	2297	-0.98
15	0.022485	0.000785	0.282195	0.000015	-17.7	1483	2297	-0.98
16	0.014609	0.000554	0.282263	0.000015	-15.2	1380	2145	-0.98
17	0.029584	0.000963	0.282195	0.000016	-17.7	1490	2298	-0.97
18	0.052725	0.002627	0.282206	0.000015	-17.4	1542	2281	-0.92
19	0.059824	0.001916	0.282253	0.000015	-15.7	1446	2174	-0.94
YL01								
Spot	$^{176}\text{Yb}/^{177}\text{Hf}$	$^{176}\text{Lu}/^{177}\text{Hf}$	$^{176}\text{Hf}/^{177}\text{Hf}$	$2\sigma$	$\epsilon_{\text{Hf}}(t)$	$T_{\text{DM1}}$ (Ma)	$T_{\text{DM2}}$ (Ma)	$f_{\text{Lu/Hf}}$
1	0.063336	0.001975	0.282228	0.000016	-16.5	1484	2227	-0.94
2	0.046178	0.001494	0.282232	0.000015	-16.3	1459	2216	-0.96
3	0.038845	0.001336	0.282223	0.000015	-16.7	1466	2235	-0.96
4	0.050535	0.001685	0.282236	0.000015	-16.2	1461	2208	-0.95
5	0.064353	0.002145	0.282225	0.000014	-16.7	1495	2235	-0.94
6	0.032743	0.001256	0.282266	0.000015	-15.1	1402	2139	-0.96
7	0.045335	0.001538	0.282272	0.000016	-14.9	1404	2128	-0.95
8	0.063873	0.002203	0.282256	0.000015	-15.6	1453	2166	-0.93
9	0.021986	0.000793	0.282195	0.000016	-17.6	1483	2295	-0.98
10	0.023385	0.000847	0.282195	0.000016	-17.6	1486	2295	-0.97
11	0.025835	0.000933	0.282197	0.000016	-17.5	1486	2291	-0.97
12	0.031725	0.001143	0.282195	0.000150	-17.6	1497	2297	-0.97
13	0.032527	0.001185	0.282194	0.000015	-17.7	1500	2299	-0.96
14	0.023337	0.000845	0.282196	0.000015	-17.6	1484	2293	-0.97
15	0.031122	0.001025	0.282195	0.000018	-17.6	1493	2296	-0.97
16	0.050063	0.001625	0.282216	0.000016	-16.9	1487	2252	-0.95
17	0.037018	0.001206	0.282217	0.000018	-16.9	1469	2248	-0.96

Continued Table 6

DL02								
Spot	$^{176}\text{Yb}/^{177}\text{Hf}$	$^{176}\text{Lu}/^{177}\text{Hf}$	$^{176}\text{Hf}/^{177}\text{Hf}$	$2\sigma$	$\varepsilon_{\text{Hf}}(t)$	$T_{\text{DM1}}$ (Ma)	$T_{\text{DM2}}$ (Ma)	$f_{\text{LwHf}}$
1	0.025803	0.000655	0.281856	0.000016	-29.8	1945	3049	-0.98
2	0.025512	0.000615	0.281863	0.000015	-29.5	1933	3034	-0.98
3	0.038622	0.000945	0.281895	0.000015	-28.4	1906	2965	-0.97
4	0.017508	0.000425	0.281845	0.000015	-30.2	1948	3073	-0.99
5	0.014914	0.000372	0.281838	0.000014	-30.4	1955	3088	-0.99
6	0.017906	0.000431	0.281885	0.000016	-28.7	1894	2985	-0.99
7	0.025411	0.000653	0.281875	0.000016	-29.1	1918	3008	-0.98
8	0.032305	0.000776	0.281875	0.000015	-29.1	1925	3008	-0.98
9	0.018508	0.000442	0.281868	0.000016	-29.3	1918	3022	-0.99
10	0.031914	0.000763	0.281856	0.000015	-29.8	1950	3050	-0.98
11	0.038503	0.000902	0.281845	0.000013	-30.2	1972	3074	-0.97
12	0.035912	0.000873	0.281843	0.000015	-30.3	1974	3079	-0.97
13	0.012521	0.000315	0.281865	0.000015	-29.4	1915	3028	-0.99
14	0.029604	0.000765	0.281843	0.000016	-30.3	1968	3078	-0.98
15	0.030813	0.000724	0.281886	0.000018	-28.7	1907	2984	-0.98
16	0.061502	0.001945	0.281873	0.000011	-29.3	1988	3017	-0.94
BS01								
Spot	$^{176}\text{Yb}/^{177}\text{Hf}$	$^{176}\text{Lu}/^{177}\text{Hf}$	$^{176}\text{Hf}/^{177}\text{Hf}$	$2\sigma$	$\varepsilon_{\text{Hf}}(t)$	$T_{\text{DM1}}$ (Ma)	$T_{\text{DM2}}$ (Ma)	$f_{\text{LwHf}}$
1	0.060314	0.001665	0.281886	0.000015	-28.8	1955	2987	-0.95
2	0.057706	0.001504	0.281873	0.000013	-29.3	1965	3015	-0.95
3	0.021505	0.000584	0.281893	0.000010	-28.5	1890	2968	-0.98
4	0.051703	0.001378	0.281873	0.000013	-29.2	1958	3015	-0.96
5	0.024015	0.000635	0.281865	0.000011	-29.5	1931	3029	-0.98
6	0.035801	0.000975	0.281885	0.000012	-28.8	1921	2987	-0.97
7	0.048904	0.001225	0.281882	0.000016	-28.9	1938	2994	-0.96
8	0.040413	0.001112	0.281892	0.000014	-28.6	1918	2972	-0.97
9	0.045802	0.001173	0.281895	0.000014	-28.5	1917	2966	-0.96
10	0.040915	0.001095	0.281888	0.000014	-28.7	1923	2981	-0.97
11	0.037506	0.001035	0.281885	0.000013	-28.8	1924	2987	-0.97
12	0.043214	0.001141	0.281875	0.000016	-29.2	1943	3009	-0.97
13	0.074122	0.002023	0.281896	0.000013	-28.5	1960	2967	-0.94
14	0.061305	0.001465	0.281903	0.000014	-28.2	1921	2949	-0.96
15	0.076513	0.001925	0.281921	0.000013	-27.6	1919	2911	-0.94
16	0.057708	0.001504	0.281843	0.000012	-30.3	2007	3081	-0.95
17	0.043203	0.001036	0.281863	0.000014	-29.6	1954	3035	-0.97

is of great significance in the study of composition, structure and dynamics of the earth (Zhou et al., 2010), it thus is closely related to the origin of mafic dykes. Nevertheless, the structure and composition of mantle transition zone is complex, which is restricted by seismic wave velocity and density and a small amount of geochemical data. Therefore, it is still difficult to determine the composition of mantle transition zone, and thus brings restriction to the investigation on the origin of the mafic dykes studied. At present, Mesozoic tectonic activity in South China can be divided into two periods (Ma and Sun, 1987; Li et al., 1997; Li, 2000; Zhang et al., 2012), and which strongly restrict the large-scale magmatic activities and mineralization in South China during the Mesozoic: 1. The Triassic was characterized by intercontinental compression folds, associated with a collisional orogeny affecting the Tethyan tectonic domain, followed by subsequent extensional deformation and magmatism (230–210 Ma). 2. During both the Middle Jurassic (175–170 Ma) and Early Cretaceous (140 Ma, 124–120 Ma, 105 Ma, and 90 Ma), strong lithospheric extension took place, which resulted in the emergence of the large number of rift basins, as well the occurrence of extensive magmatism (e.g., the emplacement of mafic dykes and A-type granite, the eruption of basalt, adakite, bimodal volcanic rock, and the development of complex, metamorphic core complexes); large-scale mineralization

in extensional setting is also a key product of these activities found across South China (Guo et al., 2001; Deng et al., 2003; Dai et al., 2005; Yan et al., 2005; Dai, 2007; Shen et al., 2008; Wang et al., 2008; Xu et al., 2009; Duan et al., 2011; Li et al., 2012; Qi et al., 2012; Zhang et al., 2012; Qi et al., 2012, 2016; Liu et al., 2012d, 2013; Xia et al., 2015; Cen et al., 2016; Zeng et al., 2016; Wang et al., 2005b, 2016; Pan et al., 2018).

Previous studies have shown that subsequent plate convergence during the Indosinian, South China was affected by oblique subduction-dominated tectonics at about 175 Ma, relating to the paleo-Pacific Plate (Deng et al., 2003). Due to the continuous subduction of the Pacific oceanic plate, the lithosphere beneath South China became thickened. Subsequently, with a change of subduction angle from low to high angled for the descending oceanic crust, there resulted the retreat of trenches, and further extension of the thickened continental lithosphere, leading to its collapse. Thus, the continental tectonic system of South China changed from dominantly one of compressional tectonics throughout the Middle–Late Jurassic to one of extensional tectonics in the Early Cretaceous (i.e., one that encompassed lithospheric extension, lithospheric subduction and underplating of mafic magmas, as well as back-arc rifting). Based upon the above discussion and the evidence provided from this study, we propose that the WMGL mafic dykes studied

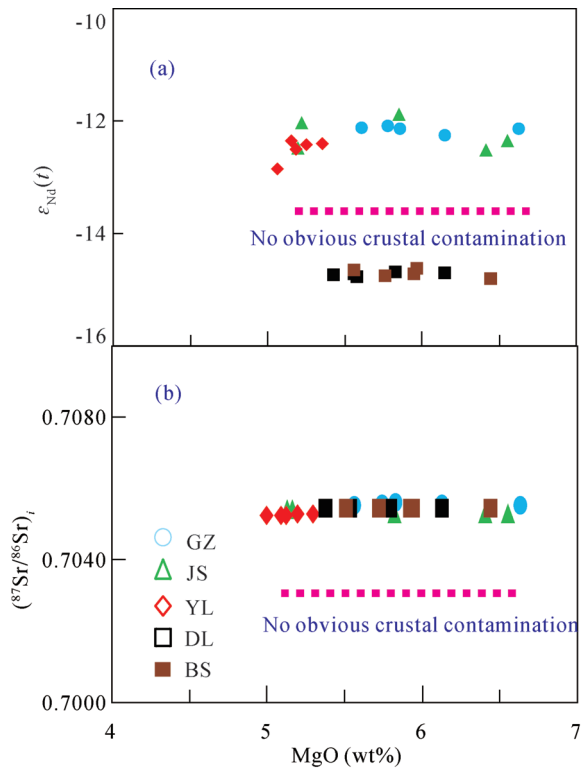


Fig. 9.  $\epsilon_{Nd}(t)$  (a) and  $(^{87}\text{Sr}/^{86}\text{Sr})_i$  (b) vs. MgO for the mafic dykes.

were most likely derived through the partial melting of an enriched mantle source. A model to explain the origin of these mafic dykes, however, is still needed. We envisage the following scenario to account for the genetic model of the mafic dykes as studied from the southern WMGL. At about 175 Ma, low-angle subduction and collision between paleo-Pacific Plate and South China resulted in crustal and lithospheric thickening (Fig. 11a); subsequently, break-off of the subducting oceanic plate occurred, which induced asthenospheric upwelling, and further lithospheric extension (Fig. 12b). The elevated heat flow from this asthenospheric mantle triggered low-degree melting (1.0%–10%) of the pre-existing enriched lithospheric mantle in this area, resulting in the production of parental basaltic magmas. Minor fractionation during ascent and emplacement of the parental magmas (i.e., fractional crystallization of phases including olivine, clinopyroxene, plagioclase, Ti-bearing phases) resulted in the widespread intrusion of dykes of mafic rock/dolerite across the WMGL, around 132–121 Ma (Fig. 11c). This genetic model is further supported by the enrichment of LILEs (i.e., Rb, Ba, Th, U, Pb, and Sr) and depletion in Nb and Ta (Fig. 5b; Dai et al., 2005; Dai, 2007) in these rocks. Nevertheless, there is no obvious crustal contamination in the process of rock formation.

## 6 Conclusions

Integrated zircon U-Pb age-dating, whole-rock elemental and Sr-Nd-Pb-Hf isotopic studies of suites of Mesozoic mafic dykes from the southern region of the

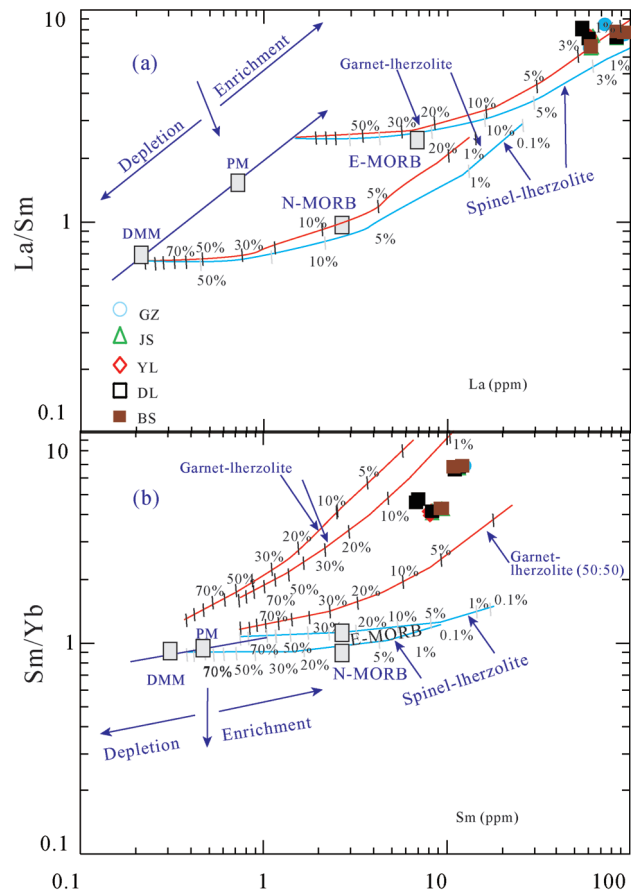


Fig. 10. La vs. La/Sm (a) and Sm vs. Sm/Yb diagrams for the mafic dykes.

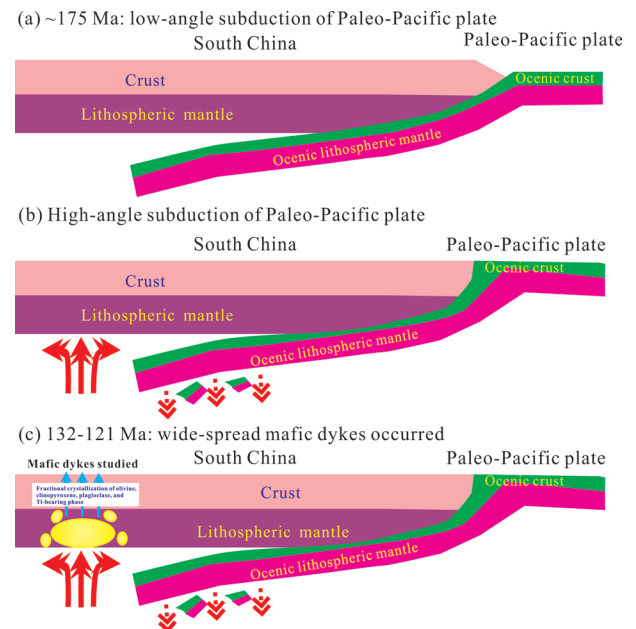


Fig. 11. The genetic model of the mafic dykes as studied from the southern WMGL

(a) low-angle subduction and collision between paleo-Pacific Plate and South China resulted in crustal and lithospheric thickening; (b) break-off of the subducting oceanic plate occurred, which induced asthenospheric upwelling, and further lithospheric extension; and (c) the genetic process for the mafic dykes studied.

WMGL allow us to draw the following conclusions.

(1) The mafic/dolerite dykes from the WMGL area were intruded during the Early Cretaceous as evidenced in the newly determined zircon U-Pb geochronological ages, of between  $131.5 \pm 1.2$  and  $121.6 \pm 1.1$  Ma.

(2) All of the sampled dolerite dykes have an affinity to alkaline and shoshonitic igneous suites. These are enriched in LREE, and select LILE (e.g., Rb, Ba, and Sr), Th, U, and Pb, and depleted in Nb, Ta, Hf, and Ti relative to primitive mantle. They have high initial  $^{87}\text{Sr}/^{86}\text{Sr}$  ratios (0.7055–0.7057), negative  $\varepsilon_{\text{Nd}}(t)$  values (–14.8 to –11.9), relatively constant Pb isotopic ratios (that are EM1-like,  $(^{206}\text{Pb}/^{204}\text{Pb})_i = 16.77\text{--}16.94$ ,  $(^{207}\text{Pb}/^{204}\text{Pb})_i = 15.43\text{--}15.47$ ,  $(^{208}\text{Pb}/^{204}\text{Pb})_i = 36.84\text{--}36.92$ ), and negative  $\varepsilon_{\text{Hf}}(t)$  values of between –30.4 and –14.9. These data suggest that the magmas parental to dolerite were generated as low degree partial melts (1.0%–10%) of an EM1-like garnet lherzolite mantle source. Minor fractionation of olivine, clinopyroxene, plagioclase, and Ti-bearing phases occurred during magma ascent, with negligible crustal contamination.

(3) Based upon this study, we propose that the swarm of mafic dyke swarm (132–121 Ma) associated with the southern region of the WMGL formed in response to asthenospheric upwelling, lithospheric extension and partial melting of lithosphere, due to subduction and subsequent slab break-off of the paleo-Pacific Ocean Plate.

## Acknowledgments

The authors thank Dr. Yang Shuqin for assistance during the XRF analyses, Prof. Qi Liang and Li Xiaobiao for assistance during ICP-MS analyses, the technician for assistance during TIMS Sr–Nd–Pb isotopic analyses, and Profs. Xiaoming Liu and Honglin Yuan for assistance during LA-ICP-MS U–Pb dating and Hf isotopic analyses. This study was supported by the National Natural Science Foundation of China (grant, 41573022).

Manuscript received May 28, 2019

accepted Jan. 2, 2020

associate EIC: CHI Guoxiang

edited by FEI Hongcai

## References

- Bai, D.Y., Huang, J.Z., Li, J.D., Wang, X.H., Ma, T.Q., Zhang, X.Y., and Chen, B.H., 2007. Mesozoic tectonic evolution of south China: Apocalypse of the Mesozoic geological evolution in southeastern Hunan and the Hunan–Guangdong–Jiangxi border area. *Geotectonica et Metallogica*, 31: 1–13 (in Chinese with English abstract).
- Bai, D.Y., Huang, J.Z., Liu, Y.R., Wu, G.Y., Ma, T.Q., and Wang, X.H., 2005. Framework of Mesozoic tectonic evolution in southeastern Hunan and the Hunan–Guangdong–Jiangxi border area. *Geology in China*, 32: 557–570 (in Chinese with English abstract).
- Barry, T.L., and Kent, R.W., 1998. Cenozoic magmatism in Mongolia and the origin of central and East Asian basalts. In: Flower, M.F.J., Chung S.L., Lo, C.H., and Lee T.Y. (eds.), *Mantle Dynamics and plate interactions in East Asia*. American Geophysical Union–Geodynamics series, 27: 347–364.
- BGMRHP (Bureau of Geology and Mineral Resources of Hunan Province), 1988. *Regional Geological Records of Hunan Province*. Beijing: Geological Publishing House (in Chinese with English abstract).
- BGMRGZAR (Bureau of Geology and Mineral Resources of Guangxi Zhuang Autonomous Region), 1985. *Regional Geological Records of Guangxi Zhuang Autonomous Region*. Beijing: Geological Publishing House (in Chinese with English abstract).
- Cai, J.H., Yan, G.H., Xiao, C.D., Wang, G.Y., and Mu, B.L., 2004. Nd, Sr, Pb isotopic characteristics of the Mesozoic intrusive rocks in the Taihang–Da Hinggan Mountains tectonomagmatic belt and their source region. *Acta Petrologica Sinica*, 20: 1225–124 (in Chinese with English abstract).
- Cen, T., Li, W.X., Wang, X.C., Pang, C.J., Li, Z.X., Xing, G.F., Zhao, X.L., and Tao, J.H., 2016. Petrogenesis of early Jurassic basalts in southern Jiangxi province, south China: implications for the thermal state of the Mesozoic mantle beneath south China. *Lithos*, 256–257: 311–330.
- Charvet, J., Shu, L.S., Shi, Y.S., Guo, L.Z., and Faure, M., 1996. The building of South China, collision of Yangzi and Cathaysia blocks, problems and tentative answers. *Journal of Southeast Asian Earth Sciences*, 13: 223–235.
- Chen, J.F., Jahn, B.M., 1998. Crustal evolution of south eastern China: Nd and Sr isotopic evidence. *Tectonophysics*, 284: 101–133.
- Chen, Y.C., Wang, D.H., Xu, Z.G., and Huang, F., 2014. Outline of regional metallogeny of ore deposits associated with the Mesozoic magmatism in south China. *Geotectonica et Metallogenia*, 38: 219–229 (in Chinese with English abstract).
- Chu, N.C., Taylor, R.N., Chavagnac, V., Nesbitt, R.W., Boella, R.M., Milton, J.A., Germain, C.R., Bayon, G., and Burton, K., 2002. Hf isotope ratio analysis using multi-collector inductively coupled plasma mass spectrometry, an evaluation of isobaric interference corrections. *Journal of Analytical Atomic Spectrometry*, 17: 1567–1574.
- Cochran, J.R., and Talwani, M., 1977. Free-air gravity anomalies in the world's oceans and their relationship to residual elevation. *Geophysical Journal of the Royal Astronomical Society*, 50: 495.
- Dai, B.Z., 2007. *Isotope Chronology and Geochemistry of Mesozoic Basic Magmatic Activities in Southern Hunan*. PhD Dissertation of Nanjing University (in Chinese with English abstract).
- Dar, B.Z., Jie, S.Y., Zhao, K.D., and Gao, J.F., 2005. Boron and its isotopes in the subduction zone: A preliminary study of Mesozoic basalts in southeast China. *Acta Geoscientica Sinica*, 26: 105–108 (in Chinese with English abstract).
- Deng, P., Shu, L.S., Tan, Z.Z., Yu, X.Q., and Wang, B., 2003. Early–Middle Jurassic basins and features of volcanic rocks in the Western Fujian–Southern Jiangxi Region. *Uranium Geology of South China*, 20: 1–17 (in Chinese with English abstract).
- Dons, S.W., Zhang, Y.Q., Hu, J.M., Zhang, Z.Y., Li, J.H., Wu, H.L., Tian, M., Chen, H., Wu, G.L., and Li, H.L., 2010. The tectonic stress field in the Dabashan Orogen resulting from Late Mesozoic intra-continental orogeny. *Acta Geoscientica Sinica*, 31: 769–780 (in Chinese with English abstract).
- Dong, S.W., Zhang, Y.Q., Long, C.X., Yang, Z.Y., Ji, Q., Wang, T., Hu, J.M., and Chen, X.H., 2008. Jurassic Tectonic revolution in China and new interpretation of the “Yanshan Movement”. *Acta Geologica Sinica (English Edition)*, 82(2): 334–347.
- Du, X.D., Xue, L.F., and Wu, G.H., 1999. Distribution of Mesozoic basin and discussion Geodynamics of continent interior in the eastern China. *Journal of Chengchun University of Science and Technology*, 39: 138–143 (in Chinese with English abstract).
- Duan, R.C., Ling, W.L., Li, Q., Chen, Z.W., Yang, H.M., and Liu, L.F., 2011. Correlations of the late Yanshanian tectonomagmatic events with metallogenesis in south China: Geochemical constraints from the Longtoushan gold ore deposit of the Dayaoshan area, Guangxi province. *Acta Geologica Sinica*, 85(10): 1644–1658 (in Chinese with English abstract).
- Ernst, E., Buchan, K.L., and Palmer, H.C. 1995. Giant dyke

- swarms, characteristics, distribution and geotectonic applications. In: Baer, G., and Heimann, A.A. (eds.) *Physics and Chemistry of Dykes*. Balkema, Rotterdam, 3–21.
- Fan, W.M., Wang, Y.J., Guo, F., and Peng, T.P., 2003. Mesozoic mafic magmatism in Hunan–Jiangxi provinces and the lithospheric extension. *Earth Science Frontiers*, 10: 159–169 (in Chinese with English abstract).
- Feng, J.P., Ouyang, Z.J., Feng, H.Y., Fan, M.M., and Ma, J., 2020. U–Pb chronology, geochemical characteristics and significance of the Taojiyao basic dike swarms in the Zhongtiao Mountain, southeastern margin of North China Craton. *Acta Geologica Sinica*, 94(2): 573–586 (in Chinese with English abstract).
- Feng, G.Y., Liu, S., Zhong, H., Feng, C., Coulson, I.M., Qi, Y., Yang, Y., and Yang, C., 2012. U–Pb zircon geochronology, geochemical, and Sr–Nd isotopic constraints on the age and origin of basaltic porphyries from western Liaoning Province, China. *International Geology Review*, 54: 1052–1070.
- Gao, X., Li, J.C., Yuan, G.L., Wang, G.H., Liang, X., Zheng, Y.L., and Wang, Q., 2019. Middle–Late Triassic magmatic records for the accretionary processes of South Qiangtang accretionary terrane, the mafic dykes in Mayigangri–Jiaomuri area, north Tibet. *Acta Petrologica Sinica*, 35: 760–774 (in Chinese with English abstract).
- Ge, X.H., Liu, J.L., Ren, S.M., and Yuan, S.H., 2014. The formation and evolution of the Mesozoic–Cenozoic continental tectonic in eastern China. *Geology in China*, 41: 19–38 (in Chinese with English abstract).
- Gilder, S.A., Keller, G.R., Luo, M., and Goodell, P.C. 1991. Timing and spatial distribution of rifting in China. *Tectonophysics*, 197: 25–243.
- Guo, X.S., Chen, J.F., Zhang, X., Tang, J.F., Xie, Z., Zhou, T.X., and Liu, Y.L., 2001. Nd isotopic ratios of K-enriched magmatic complexes from southeastern Guangxi province: implications for upwelling of the mantle in southeastern China during the Mesozoic. *Acta Petrologica Sinica*, 17: 19–27.
- Halls, H.C., 1982. The importance and potential of mafic dyke swarms in studies of geodynamic process. *Geosciences Canada*, 9: 145–154.
- Halls, H.C., and Fahrig, W.E., 1987. Mafic dyke swarms. Geological Association of Canada, Special paper, 34: 503
- Harris, A.C., Allen, C.M., Bryan, S.E., Compbell, I.H., Holcombe, R.J., and Palin, J.M., 2004. ELAICPMS UPb zircon geochronology of regional volcanism hosting the Bajo de la Alumbrera CuAu deposits, implications for porphyry-related mineralization. *Mineralium Deposita*, 39: 46–67.
- Hart, S.R., 1984. A large-scale isotope anomaly in the southern Hemisphere mantle. *Nature*, 309: 753–757.
- Hilde, T.W.C., Uyede, S., and Kroenke, L., 1977. Evolution of the western pacific and its margin. *Tectonophysics*, 38: 145–165.
- Hirajima, T., Ishiwatari, A., Cong, B., Zhang, R., Banno, S., and Nozaka, T., 1990. Coesite from Mengzhong eclogite at Donghai county, northern Jiangsu Province. *Mineralogical Magazine*, 54: 579–583.
- Hou, G.Q., 2012. Mafic dyke swarms of North China. Beijing: Science Press (in Chinese with English abstract).
- Hou, G.T., Liu, Y.L., and Li, J.H., 2006. Evidence for 1.8 Ga extension of the Eastern Block of the North China Craton from SHRIMP U–Pb dating of mafic dyke swarms in Shandong Province. *Journal of Asian Earth Sciences*, 27: 392–401.
- Hou, G.T., and Mu, Z.G., 1994. K–Ar ages and their geological significance of late Precambrian mafic dyke swarms in the North China Craton. *Journal of Geology & Mineral Research North China*, 9: 267–270 (in Chinese with English abstract).
- Hu, R.Z., Bi, X.W., Peng, J.T., Liu, S., Zhong, H., Zhao, J.H., and Jiang, G.H., 2007. Some problems concerning relationship between Mesozoic–Cenozoic lithospheric extension and uranium metallogenesis in South China. *Mineral Deposits*, 26: 139–151 (in Chinese with English abstract).
- Hu, R.Z., Mao, J.W., Hua, R.M., and Fan, W.M., 2015. Intercontinental mineralization of south china continental block. Beijing: Science Press (in Chinese).
- Huang, J.P., Fu, R.S., Zheng, Y., Xu, T.H., Liu, X., and Han, L.B., 2008. The influence of mantle convection to the lithosphere deformation of China mainland. *Chinese Journal of Geophysics*, 51: 1048–1057 (in Chinese with English abstract).
- Huang, P.H., and Fu, R.S., 1982. Mantle convection pattern under lithosphere of China. *Acta Geophysica Sinica*, 26: 39–47 (in Chinese with English abstract).
- Huang, R., Zhu, L.P., and Xu, Y.X., 2014. Crustal structure of Hubei province of China from teleseismic receiver functions, Evidence for lower crust delamination. *Tectonophysics*, 636: 286–292.
- Ji, W.B., 2014. Late Mesozoic extensional structures in South China and their response to the destruction of the North China Craton. Ph.D. Dissertation of Chinese Academy of Sciences (in Chinese with English abstract).
- Jia, D.C., 2003. Geochemistry and lithospheric evolution of Mesozoic basic rocks in eastern Hunan and Guangxi. Post-doctoral outbound report of Institute of geochemistry, Chinese Academy of Sciences (in Chinese with English abstract).
- Jia, D.C., Hu, R.Z., Lu, Y., and Xie, G.Q., 2002a. Petrological and geochemical characteristics of strontium-rich lamprophyres from Jiaoxiling in northeast Hunan province. *Acta Petrologica Sinica*, 18: 459–467 (in Chinese with English abstract).
- Jia, D.C., Hu, R.Z., and Xie, G.Q., 2002b. Trace element geochemical characteristics and genesis of Mesozoic mafic dikes in Northeast Hunan province. *Geology Geochemistry*, 30: 33–39 (in Chinese with English abstract).
- Jia, D.C., Hu, R.Z., and Xie, G.Q., 2002c. Petrological geochemistry of the Mesozoic mafic dikes and their implication on tectonic setting in northeast Hunan province. *Geotectonic et Metallogenia*, 26: 179–184 (in Chinese with English abstract).
- Johnson, K.T.M., 1998. Experimental determination of partition coefficients for rare earth and high-field-strength elements between clinopyroxene, garnet, and basaltic melt at high pressure. *Contributions to Mineralogy and Petrology*, 133: 60–68.
- Le Maitre, R.W., 2002. *Igneous rocks, A classification and glossary of Terms*, 2nd. Cambridge University Press, Cambridge, UK, 236.
- Li, J.H., Hou, G.Q., Qian, X.L., Halls, H.C., and Davis, D., 2001. Single-zircon U–Pb age of the initial Mesoproterozoic basic dike swarms in Hengshan Mountain and its implication for the tectonic evolution of the North China Craton. *Geological Reviews*, 47: 234–238 (in Chinese with English abstract).
- Li, X.H., 2000. Cretaceous magmatism and lithospheric extension in southeast China. *Journal of Asian Earth Sciences*, 18: 293–305.
- Li, X.H., Chung, S.L., Zhou, H.W., Lo, C.H., Liu, Y., and Chen, C.H., 2004. Jurassic interpolate magmatism in southern Hunan–eastern Guangxi,  $^{40}\text{Ar}/^{39}\text{Ar}$  dating, geochemistry, Sr–Nd isotopes and implications for the tectonic evolution of SE China. Geological Society, London, Special Publication, 226: 193–215.
- Li, X.H., Hu, R.Z., and Rao, B., 1997. Geochronology and geochemistry of Cretaceous mafic dikes from northern Guangdong, SE China. *Geochimica*, 26: 14–31 (in Chinese with English abstract).
- Li, X.H., Li, Z.X., Li, W.X., Liu, Y., Yuang, C., Wei, G.J., and Qi, C.S., 2007. U–Pb zircon, geochemical and Sr–Nd–Hf isotopic constraints on age and origin of Jurassic I- and A-type granites from central Guangdong, SE China, a major igneous event in response to foundering of a subducted flat–slab? *Lithos*, 96: 186–204.
- Li, X.Z., Han, B.F., Ji, J.Q., Li, Z.H., and Yang, B., 2004. Geology, geochemistry and K–Ar ages of the Karamay basic–intermediate dyke swarm from Xinjiang, China. *Geochimica*, 33: 574–584 (in Chinese with English abstract).
- Li, X.Z., Han, B.F., Li, Z.H., Liu, Z.Q., and Du, W., 2005. Mechanism of the Karamay basic–intermediate dyke swarm from Xinjiang and tectonic implications. *Geological Review*, 51: 517–522 (in Chinese with English abstract).
- Li, Z., Qiu, J.S., and Xu, X.S., 2012. Geochronological,

- geochemical and Sr-Nd-Hf isotopic constraints on petrogenesis of late Mesozoic gabbro-granite complexes on the southeast coast of Fujian, south China: insights into a depleted mantle source region and crust-mantle interactions. *Geological Magazine*, 149: 459–482.
- Li, Z.W., and Yang, S.X., 1988. Basic characteristics of the tectonic stress field in south China since the Mesozoic era. *Journal of Seismological Research*, 11: 59–66 (in Chinese with English abstract).
- Li, Z.X., and Li, X.H., 2007. Formation of the 1300-km-wide intracontinental orogen and post orogenic magmatic province in Mesozoic South China, A flat-slab subduction model. *Geology*, 35: 179–182.
- Lin, Y., Tang, Q.Y., Zhang, M.J., Jia, J.G., Chen, S.T., and Hu, X., 2014. Magmatism and dynamic settings of Permian mafic dyke swarms in the northern of Xinjiang. *Journal of Earth Sciences and Environment*, 36: 73–82 (in Chinese with English abstract).
- Liu, C.Z., Liu, Z.C., Wu, F.Y., and Chu, Z.Y., 2012d. Mesozoic accretion of juvenile sub-continental lithospheric mantle beneath south China and its implications: geochemical and Re-Os isotopic results from Ningyuan mantle xenoliths. *Chemical Geology*, 291: 186–198.
- Liu, G.J., 1994. *Geophysical and geological atlas of China Sea and its adjacent areas*. Beijing: Geological Publishing House (in Chinese).
- Liu, Q.Y., He, L.J., and Huang, F., 2013. Review of Mesozoic geodynamics research of south China. *Progress in Geophysics*, 28: 633–647 (in Chinese with English abstract).
- Liu, S., 2004. *Mesozoic Magmatism and Crustal Extension in Shandong Province and the Relation between Lamprophyre and Gold Mineralization*. PhD dissertation, Institute of Geochemistry, Chinese Academy of Sciences (in Chinese with English abstract).
- Liu, S., Feng, C., Feng, G., Xu, M., Coulson, I.M., Guo, X., Guo, Z., Peng, H., and Feng, Q., 2017. Timing, mantle source and origin of mafic dykes within the gravity anomaly belt of the Taihang-Da Hinggan gravity lineament, central North China Craton. *Journal of Geodynamics*, 109: 41–58.
- Liu, S., Feng, C., Santosh, M., Feng, G., Coulson, I.M., Xu, M., Guo, Z., Guo, X., Peng, H., and Feng, Q., 2018. Integrated elemental and Sr-Nd-Pb-Hf isotopic studies of Mesozoic mafic dykes from the eastern North China Craton, implications for the dramatic transformation of lithospheric mantle. *Journal of Geodynamics*, 114: 19–40.
- Liu, S., Hu, R.-Z., Gao, S., Feng, C.-X., Qi, L., Zhong, H., Xiao, T., Qi, Y.-Q., Wang, T., and Coulson, I.M., 2008a. Zircon U-Pb geochronology and major, trace elemental and Sr-Nd-Pb isotopic geochemistry of mafic dykes in western Shandong Province, east China, constrains on their petrogenesis and geodynamic significance. *Chemical Geology*, 255: 329–345.
- Liu, S., Hu, R., Gao, S., Feng, C., Qi, Y., Wang, T., Feng, G., and Coulson, I.M., 2008b. U-Pb zircon age, geochemical and Sr-Nd-Pb-Hf isotopic constraints on age and origin of alkaline intrusions and associated mafic dikes from Sulu orogenic belt, Eastern China. *Lithos*, 106: 365–379.
- Liu, S., Hu, R., Gao, S., Feng, C., Yu, B., Feng, G., Qi, Y., Wang, T., and Coulson, I.M., 2009. Petrogenesis of Late Mesozoic mafic dykes in the Jiaodong Peninsula, eastern North China Craton and implications for the foundering of lower crust. *Lithos*, 113: 621–639.
- Liu, Z.P., Gao, X.L., and Li, Y.S., 2003. Density structure of the Taihang mountains gravity anomaly zone and its geological interpretation. *Seismology and Geology*, 25: 266–272 (in Chinese with English abstract).
- Lizuka, T., and Hirata, T., 2005. Improvements of precision and accuracy in in-situ Hf isotope microanalysis of zircon using the laser ablation-MC-ICPMS technique. *Chemical Geology*, 220: 121–137.
- Long, Q., 2017. *Geochemistry of Mesozoic petroclastic wall in Jiaodong area*. PhD. thesis of University of Science and Technology of China (in Chinese with English abstract).
- Lu, X.C., Hu, W.X., and Gu, L.X., 1998. Mantle convection and its impact on the extending basins. *Earth Science Frontiers*, 184–190 (in Chinese with English abstract).
- Luo, M.S., Lu, L.Q., Jia, J., Wang, S.D., Xu, Y.D., and He, W.H., 2014. Evolution of sedimentary basins in China during Mesozoic. *Journal of China University of Geosciences*, 39: 954–976 (in Chinese with English abstract).
- Ma, K.Y., and Sun, D.M., 1987. The tectonic significance of Wulingshan gravity gradient zone. *Bulletin of the Institute of Mineral Deposits*, 2: 135–141 (in Chinese with English abstract).
- Ma, X.Y., 1987. *The Key Points of Lithospheric Dynamics in China*. Beijing: Geological Publishing House (in Chinese).
- Ma, Z.J., Gao, X.L., and Song, Z.F., 2006. Analysis and tectonic interpretation to the horizontal-gradient map calculated from Bouguer gravity data in the China mainland. *Chinese Journal of Geophysics*, 49: 106–114 (in Chinese).
- Machado, N., and Simonetti, A., 2001. U-Pb dating and Hf isotopic composition of zircon by laser-ablation MC-ICP-MS. In: Sylvester, P. (ed.), *Laser Ablation-ICPMS in the Earth Science, principles and applications*, Mineralogical Association of Canada Short Course Series 29: 121–146.
- Mao, J.R., Li, Z.L., and Ye, H.M., 2014. Mesozoic tectonic-magmatic activities in South China, current situation and prospects. *Science in China (D)*, 44: 2593–22617 (in Chinese).
- Mao, J.W., Xie, G.Q., and Cheng, Y.B., Chen, Y.K., 2009. Mineral deposit models of Mesozoic ore deposits in south China. *Geological Review*, 55: 347–354 (in Chinese with English abstract).
- Mao, J.W., Xie, G.Q., Li, X.F., Zhang, C.Q., and Mei, Y.X., 2004. Mesozoic large scale mineralization and multiple lithospheric extensions in South China. *Earth Science Frontiers*, 11: 45–55 (in Chinese with English abstract).
- Middlemost, E.A.K., 1994. Naming materials in the magma/igneous rock system. *Earth-Science Reviews*, 74: 193–227.
- Molnar, P., and Tapponnier, P., 1975. Cenozoic tectonics of Asia, effects of continental collision. *Science*, 189: 419–426.
- Niu, Y.L., 2005. Great debate on mantle plume. *Chinese Science Bulletin*, 50: 1797–1800 (in Chinese).
- Pan, F.B., Jin C., Jia, B.J., Liu, R., He, X.B., Gao, Z., Tao, L., Zhou, X.C., and Zhang, L.Q., 2018. A late Mesozoic short-lived shift from fluid-dominated to sediment-dominated mantle metasomatism in the northeast south China Block and its tectonic implications. *Lithos*, 288–301.
- Peng, P., Bleeker, W., Ernst, R.E., Söderlund, U., and McNicoll, V., 2011a. U-Pb baddeleyite ages, distribution and geochemistry of 925 Ma mafic dykes and 900 Ma sills in the North China craton, evidence for a Neoproterozoic mantle plume. *Lithos*, 127: 210–221.
- Peng, P., Guo, J.H., Zhai, M.G., and Bleeker, W., 2010. Paleoproterozoic gabbro noritic and granitic magmatism in the northern margin of the North China Craton, evidence of crust-mantle interaction. *Precambrian Research*, 183: 635–659.
- Peng, P., Zhai, M.G., Guo, J.H., Kusky, T., and Zhao, T.P. 2007. Nature of mantle source contributions and crystal differentiation in the petrogenesis of the 1.78 Ga mafic dykes in the central North China craton. *Gondwana Research*, 12: 29–46.
- Peng, P., Zhai, M.G., Li, Q.L., Wu, F.Y., Hou, Q.L., Li, Z., Li, T.S., and Zhang, Y.B., 2011b. Neoproterozoic (900 Ma) Sariwon sills in North Korea, geochronology, geochemistry and implications for the evolution of the south-eastern margin of the North China Craton. *Gondwana Research*, 20: 243–254.
- Peng, P., Zhai, M.G., Li, Z., Wu, F.Y., and Hou, Q.L. 2008. Neoproterozoic (~820 Ma) mafic dyke swarms in the North China craton, implication for a conjoint to the Rodinia supercontinent? Abstracts, 13th Gondwana Conference, Dali, China, 160–161.
- Peng, P., Zhai, M.G., and Zhang, H.F., Guo, J.H. 2005. Geochronological constraints on the Palaeoproterozoic evolution of the North China Craton, SHRIMP zircon ages of different types of mafic dykes. *International Geology Review*, 47: 492–508.
- Qi, L., Hu, J., and Gregoire, D.C., 2000. Determination of trace elements in granites by inductively coupled plasma mass spectrometry. *Talanta*, 51: 507–513.
- Qi, Y.Q., Hu, R., Liu, S., Coulson, I.M., Qi, H.W., Tian, J.J.,

- Feng, C., and Wang, T., 2012. Geochemical and Sr–Nd–Pb isotopic compositions of Mesozoic mafic dikes from the Gan–Hang tectonic belt, south China: Petrogenesis and geodynamic significance. *International Geology Review*, 54, 920–939.
- Qi, Y.Q., Hu, R., Liu, S., Coulson, I.M., Qi, H.W., Tian, J.J., Feng, C., Wang, T., Zhu, J., and Chen, H., 2016. Petrogenesis and geodynamic setting of Early Cretaceous mafic–ultramafic intrusions, South China, A case study from the Gan–Hang tectonic belt. *Lithos*, 258–259: 149–162.
- Ren, J.S., 1990. On the geotectonic of southern China. *Acta Geologica Sinica*, 64(2): 275–288 (in Chinese with English abstract).
- Ren, J.S., Chen, T.Y., and Niu, B.G., 1992. Tectonic evolution and metallogenesis of continental lithosphere in eastern China and its adjacent areas. Beijing: Science Press (in Chinese).
- Rodger, J., 1989. Comments on “Mesozoic overthrust tectonics in south China”. *Geology*, 17: 671–672.
- Rowley, D.B., Ziegler, A.M., and Nie, G., 1989. Comment on “Mesozoic overthrust tectonics in south China”. *Geology*, 7: 384–386.
- Rudnick, R.L., Fountain, D.M., 1995. Nature and composition of the continental crust, a lower crustal perspective. *Reviews in Geophysics*, 33: 267–309.
- Shao, J.A., Zhai, M.G., Zhang, L.Q., and Li, D.M., 2005. Identification of 5 time–group of dike swarms in Shanxi–Hebei–Inner Mongolia border area and its tectonic implications. *Acta Geologica Sinica*, 79(1): 56–67 (in Chinese with English abstract).
- Shao, J.A., and Zhang, L.Q., 2002. Mesozoic dyke swarms in the north of North China. *Acta Petrologica Sinica*, 18: 312–318 (in Chinese with English abstract).
- Shao, R.S., 2001. Genesis of Mesozoic–Cenozoic Faulted Red Basin in Eastern South China. M.Sc. thesis, Sun Yat–sen University (in Chinese with English abstract).
- Shen, X.M., Zhang, H.X., and Zhang, B.Y., 2008. A preliminary study of relationship between metamorphic core complexes and lithospheric thinning over the Mesozoic in south China. *Geotectonica et Metallogenia*, 32: 11–19 (in Chinese with English abstract).
- Shu, L.S., 2012. An analysis of principal features of tectonic evolution in south China block. *Geological Bulletin of China*, 31: 1035–1053 (in Chinese with English abstract).
- Shu, L.S., Zhou, X.M., Deng, P., Yu, X.Q., Wang, B., and Zu, F.P., 2004. Geological features and tectonic evolution of Mesozoic–Cenozoic basins in southeastern China. *Geological Bulletin of China*, 23: 876–884 (in Chinese with English abstract).
- Sun, S.S., and McDonough, W.F., 1989. Chemical and isotopic systematic of oceanic basalts, Implications for mantle composition and processes. In: Saunders A.D., and Norry, M.J. (eds.), *Magmatism in the Ocean basins*. Geol. Society Spec. Pub. 42: London, 313–345.
- Tapponnier, P., and Molnar, P., 1976. Slip–ling field theory and large–scale Continental tectonics. *Nature*, 264: 318–324.
- Tang, L., 2013. Geochronology and geochemistry of Mesozoic basic dykes and acidic rocks in Hebei and Inner Mongolia. M.Sc. thesis, Institute of geochemistry, Chinese Academy of Sciences (in Chinese with English abstract).
- Tu, G.C., Gao, Z.M., and Cheng, J.M., 1998. Cryogenic geochemistry. Beijing: Science Press (in Chinese).
- Tu, G.C., Liu, B.G., Li, C.Y., Wang, X.Z., and Zhao, Z.H., 2000. *Super Large Deposits in China (I)*. Beijing: Science Press (in Chinese).
- Uyeda, S.A., and Miyashiro, A., 1974. Plate, tectonics and Japanese Islands. *Bulletin of the Geological Society of America*, 85: 1159–1170.
- Wan, T.F., 1993. Mesozoic–Cenozoic intraplate deformation tectonic stress field in eastern China and its application. Beijing: Geological Publishing House (in Chinese).
- Wan, T.F., Wang, Y.M., and Liu, J.L., 2008. Detachments and magmatic source depth in lithosphere of eastern China during Yanshanian and Sichuanian stages. *Earth Science Frontiers*, 15: 1–35.
- Wang, S., Zhang, D., Wu, G.G., Vatuva, A., Di, Y.J., Yan, P.C., Feng, H.B., and Ma, S., 2016. Late Paleozoic to Mesozoic extension in southwestern Fujian province, south China: geochemical, geochronological and Hf isotopic constraints from basic–intermediate dykes. *Geoscience Frontiers*, 1–12.
- Wang, D.Z., 2004. The study of granitic rocks in south China, looking back and forward. *Geological Journal of China Universities*, 10: 305–314 (in Chinese with English abstract).
- Wang, Q., Zhao, Z.H., Jian, P., Xiong, X.L., Bao, Z.W., Dai, T.M., Xu, J.F., and Ma, J.L., 2005. Geochronology of Cretaceous A-type granitoids or alkaline intrusive rocks in the hinterland, south China, constraints for late–Mesozoic tectonic evolution. *Acta Petrologica Sinica*, 21: 795–808 (in Chinese with English abstract).
- Wang, S.Y., Xu, Z.H., Y and u, Y.X., 1996. Inversion for the plate driving forces acting at the boundaries of China and its surroundings. *Acta Geophysica Sinica*, 764–771 (in Chinese with English abstract).
- Wang, X.C., and Rao, B., 1989. A geological study of basic dikes in Guidong granite of northern Guangdong Province. *Journal of Nanjing University*, 25: 120–131 (in Chinese with English abstract).
- Wang, Y.J., Fan, W.M., Cawood, P.A., and Li, S.Z., 2008. Sr–Nd–Pb isotopic constraints on multiple mantle domains for Mesozoic mafic rocks beneath the south China Block hinterland. *Lithos*, 106: 297–308.
- Wang, Y.J., Fan, W.M., Liang, X.Q., Peng, T.P., and Shi, Y.R., 2005a. SHRIMP zircon U–Pb geochronology of Indosinian granites in Hunan Province and its petrogenetic implications. *Chinese Science Bulletin*, 50: 1395–1403.
- Wang, Y.J., Fan, W.M., Peng, T.P., and Guo, F., 2005b. Elemental and Sr–Nd isotopic systematics of the early Mesozoic volcanic sequence in southern Jiangxi province, South China: Petrogenesis and tectonic implications. *International Journal of Earth Sciences*, 94: 53–65.
- Watson, E.B., and Harrison, T.M., 1983. Zircon saturation revisited, temperature and composition effects in a variety of crustal magma types. *Earth and Planetary Science Letters*, 64: 295–304.
- Wei, S.Y., Teng, J.W., and Wang, Q.S., 1990. *Lithospheric Structure and Dynamics in the Continental Margin of Eastern China*. Beijing: Science Press (in Chinese).
- Wood head, J., Hergt, J., Shelley, M., Eggins, S., and Kemp, R., 2004. Zircon Hf–isotope analysis with an excimer laser, depth profiling, ablation of complex geometries, and concomitant age estimation. *Chemical Geology*, 209: 121–135.
- Wu, F.Y., Walker, R.J., Yang, Y.H., Yuan, H.L., and Yang, J.H., 2006. The chemical–temporal evolution of lithospheric mantle underlying the North China Craton. *Geochimica et Cosmochimica Acta*, 70: 501–503.
- Wu, F.Y., Xu, Y.G., Gao, S., and Zheng, J.P., 2008. Lithospheric thinning and destruction of the North China Craton. *Acta Petrologica Sinica*, 24: 1145–1174 (in Chinese with English abstract).
- Wu, Z.M., and Liu, H.Q., 1985. Evaluation and evolution of the major rift valley of Meso–Cenozoic in eastern China. *Experimental Petroleum Geology*, 7: 60–69 (in Chinese with English abstract).
- Xia, S.C., Shen, Y.S., Zhao, D.P., and Qiu, X.L., 2015. Lateral variation of crustal structure and composition in the Cathaysia block of south China and its geodynamic implications. *Journal of Asian Earth Sciences*, 109: 20–28.
- Xie, G.Q., 2003. Geological and geochemical characteristics of basic dikes (body) in southeastern China since late Mesozoic and their geodynamic significance, a case study of Jiangxi. PhD dissertation, Institute of geochemistry, Chinese Academy of Sciences (in Chinese with English abstract).
- Xie, G.Q., Hu, R.Z., and Jia, D.C., 2002. Geological and geochemical characteristics and its significance of mafic dikes from northwest Jiangxi province. *Geochimica*, 31: 329–337 (in Chinese with English abstract).
- Xu, X.B., Zhang, Y.Q., Jia, D., Shu, L.S., and Wang, R.R., 2009. Early Mesozoic geotectonic processes in south China. *Geology in China*, 36: 543–593 (in Chinese with English abstract).
- Xu, Y.G., 2006. Formation of the Taihangshan Gravity lineament by the diachronous lithospheric thinning of the North China Craton. *Journal of China University of*

- Geosciences, 31: 14–22 (in Chinese with English abstract).
- Yan, J., Chen, J.F., Xie, Z., Yan, G., Yu, G., and Qian H., 2005. Geochemistry of late Mesozoic basalts from Kedoushan in the middle and lower Yangtze regions: constraints on characteristics and evolution of the lithospheric mantle. *Geochimica*, 34: 455–469 (in Chinese with English abstract).
- Yan, Y.X., 2005. Research on geochemistry and Sr, Nd and Pb isotope of the basic dyke swarms in Ziyang–Langao area, Shaanxi Province. Master's thesis of Northwest University.
- Yan, Y.X., and Ye, X.S., 1982. A preliminary study on the origin and metallogenetic characteristics of Mesozoic granites in Quangxi province. *Geochimica*, 2: 173–181 (in Chinese with English abstract).
- Yang, B.J., and Liu, W.S., 2000. Origin of gravity cascade belt in Daxing'an Mountains, Taihang Mountains and Wuling Mountains. *Journal of Changchun University of Science and Technology*, 30: 23–25 (in Chinese with English abstract).
- Yang, B.J., Mu, S.M., Jun, X., and Liu, C., 1996. Synthesized study on the geophysics of Manzhouli–Suifenhe transects, China. *Acta Geophysica Sinica*, 39: 772–782 (in Chinese with English abstract).
- Yang, C.G., 2012. Geochronological and geochemical characteristics of basic diamonds in the southern margin of north china plate. M.Sc. thesis, Institute of geochemistry, Chinese Academy of Sciences (in Chinese with English abstract).
- Yang, J.H., Chung, S.L., Zhai, M.G., and Zhou, X.H., 2004. Geochemical and Sr-Nd-Pb isotopic compositions of mafic dikes from the Jiaodong Peninsula, China, evidence for vein-plus-peridotite melting in the lithospheric mantle. *Lithos*, 73: 156–160.
- Yang, Y.H., Liu, S., Hu, R.Z., Feng, C.X., Feng, G.Y., Qi, Y.Q., and Tang, L., 2013. Geochemical feature and petrogenesis of Houcheng mafic dyke in Hebei: evidence from major and trace elements. *Geological Bulletin of China*, 32: 607–616 (in Chinese with English abstract).
- Yang, Z.R., 1988. Geotectonic significance of the regional gravitational field in China. *Geotectonic et Metallogenia*, 12: 155–164 (in Chinese with English abstract).
- Yu, X.Q., Hou, M.J., and Wang, D.E., 2005. No evidence for a large Mesozoic overthrust in the Lantian area of Anhui Province, south China. *Journal of Asian Earth Sciences*, 25: 601–609.
- Zeng, G., He, Z.Y., Li, Z., Xu, X.S., and Chen, L.H., 2016. Geodynamics of paleo-Pacific plate subduction constrained by the source lithologies of late Mesozoic basalts in southeastern China. *Geophysical Research Letters*, 43: 1–9.
- Zeng, R.S., 1984. Introduction to solid geophysics. Science Press (in Chinese).
- Zhang, G.W., Guo, A.L., Wang, Y.J., Li, S.Z., Dong, Y.P., Liu, S.F., He, D.F., Cheng, S.Y., Lu, R.K., and Yao, A.P., 2013. The continental tectonics and problems in South China. *Science in China (D)*, 43: 1553–1582 (in Chinese).
- Zhang, Y.Q., Dong, S.W., Li, J.H., Cui, J.J., Su, J.B., and Li, Y., 2012. The new progress in the study of Mesozoic tectonics of south China. *Acta Geoscientica Sinica*, 33: 257–279 (in Chinese with English abstract).
- Zhang, Y.X., 1986. Relationship of Mesozoic magmatic activity to mantle heat source in south China. *Bull. Nanjing Inst. Geol. M. R.*, Chinese Academy of Geological Sciences, 7: 53–63.
- Zhai, M.G., and Liu, W.J., 2003. Paleoproterozoic tectonic history of the North China Craton, A review. *Precambrian Research*, 122: 183–199.
- Zhang, G.S., 2006. Geochronology, Geochemistry and Geodynamic Significance of Basic-ultrabasic Rocks in Fujian Province since Late Mesozoic. PhD dissertation, Institute of geochemistry, Chinese Academy of Sciences (in Chinese with English abstract).
- Zhang, H.W., 2010. Geochemical characteristics and petrogenesis of adakitic granite in Shangcheng area, Henan province. *Geology and Mineral Resources of South China*, 4: 1–7 (in Chinese with English abstract).
- Zhang, Q.C., Wu, Z.H., Li, S., Li, K., Liu, Z.W., Zhou, Q., 2019a. Ordovician granitoids and Silurian mafic dikes in the Western Kunlun Orogen, Northwest China: Implications for evolution of the Proto-Tethys. *Acta Geologica Sinica (English Edition)*, 93(1): 30–49.
- Zhang, S.H., Zhang, R.Y., Zhou, J.Y., 2019b. LA- ICP- MS Zircon U- Pb age, geochemical characteristics of the Paleoproterozoic metamorphosed mafic dykes in Zhongtiao Mountains, Shanxi Province, and their geological implications. *Geological Review*, 65 (6): 350–1362.
- Zhang, Y.Q., Dong, S.W., Li, J.H., Cui, J.J., Shi, W., Su, J.B., and Li, Y., 2012. The new progress in the study of Mesozoic tectonics of south China. *Acta Geoscientica Sinica*, 33: 257–279 (in Chinese with English abstract).
- Zhao, J.H., 2004. Geochronology and Geochemistry of Basic Rocks in Fujian Province, Mantle Evolution in Southeast China since Late Mesozoic. PhD dissertation, Institute of geochemistry, Chinese Academy of Sciences (in Chinese with English abstract).
- Zhao, J.H., Hu, R.Z., and Liu, S., 2004. Geochemistry, petrogenesis, and tectonic significance of Mesozoic mafic dikes, Fujian Province, Southeastern China. *International Geology Review*, 6: 528–541.
- Zhou, C.Y., Jin, Z., and Zhang, J.F., 2010. Mantle transition zone: an important field in the studies of earth's interior. *Earth Science Frontiers*, 17: 90–113 (in Chinese with English abstract).
- Zhao, Y., Xu, G., Zhang, S.H., Yand, Z.Y., Zhang, Y.Q., and Hu, J.M., 2004. Yanshanian movement and conversion of tectonic regimes in East Asia. *Earth Science frontiers*, 11: 319–328 (in Chinese with English abstract).
- Zhou, J.W., 1987. Metabasic dykes groups and in which strain-slip of the Dengfeng granite-greenstone terrene in the Qishan, Henan. *Journal of Northwest University*, 17: 43–50 (in Chinese with English abstract).
- Zhou, J.W., Liu, L., Han, S., Wang, J.L., Dong, Y.P., Zhang, C.L., and Liu, Y.Y., 1997. Preliminary study on basic dyke group in Wudang Block and its geological significance. *Chinese Science Bulletin*, 42: 2546–2549 (in Chinese).
- Zhou, X.M., My thinking about granite geneses of South China. *Geological Journal of China Universities*, 9: 557–565 (in Chinese with English abstract).
- Zhou, X.M., Sun, T., Shen, W.Z., Shu, L.S., and Niu, Y.L., 2006. Petrogenesis of Mesozoic granitoids and volcanic rocks in South China, a response to tectonic evolution. *Episodes*, 29: 26–33.
- Zhou, Y.X., and Liu, W.J., 1979. Regional gravity field and its basic features in China. *Geophysical and Geochemical Exploration*, 1: 14–17.

#### About the first and corresponding author



CHEN Xiaoqing, born in 1993 in Xi'an, Shaanxi Province; graduated from Northwest University of Political Science and Law; Ph.D. Postgraduates of Jilin University. She is now interested in the study on petrology and geochemistry. Email: xqchen66@163.com; phone: 18577370425.